# *Theoretical study of an inviscid transonic flow near a discontinuity in wall curvature (Part 1)*

Yumashev, Dmitry

2012

MIMS EPrint: **2012.40**

Manchester Institute for Mathematical Sciences
School of Mathematics

The University of Manchester

Reports available from: http://eprints.maths.manchester.ac.uk/
And by contacting: The MIMS Secretary
School of Mathematics
The University of Manchester
Manchester, M13 9PL, UK

ISSN 1749-9097

# Theoretical study of an inviscid transonic flow near a discontinuity in wall curvature (Part 1)

**DMITRY YUMASHEV**[1]

[1]School of Mathematics, University of Manchester, Oxford Road, Manchester, M13 9PL, UK

(Received ?? and in revised form ??)

The work provides an extensive theoretical study of an inviscid transonic flow in the vicinity of a wall curvature discontinuity. Depending on the ratio of the curvatures upstream and downstream of the break, several physically different regimes can exist, including a special type of supersonic flows which decelerate to subsonic speeds without a shock wave, transonic Prandtl–Meyer flow and supersonic flows with a weak shock. Using a new numerical technique of solving the Karman–Guderley equation in the ODE form, we perform computations and then employ the *hodograph method* along with the *phase portrait technique* to obtain a complete theoretical description of the flow. It appears that if the flow can be extended beyond the *limiting characteristic*, it subsequently develops a shock wave. As a consequence, a fundamental link between the local and the global flow patterns is observed in our problem (a detailed description of this is given in Part 2). The curvature discontinuity leads to singular pressure gradients $\partial p/\partial x \sim G_{\mp}\,(\mp x)^{-1/3}$ upstream and downstream of the break point, respectively. Analytical expressions for the amplitude coefficients $G_{\mp}$ are derived as functions of the ratio of the curvatures. These results are important for a subsequent study of the boundary layer separation.

**Key Words:**

---

## 1. Introduction

The classical theory of transonic flows dates back to the beginning of the 20th century, and it underwent a rapid development in early 1950s, largely due to the works of Frankl (1947) and Guderley (1957). A summary of the main theoretical results in this area and the key references may be found in the monograph by Cole & Cook (1986). Guderley (1957) introduced an important technique of analysing the singular points of the non-linear Karman–Guderley equations by considering the so-called *phase portrait* of a transonic flow. Combined with the *hodograph method* proposed by Chaplygin (1902) in his famous study of compressible jets, this technique provides a powerful tool for investigating various special cases such as the transonic far-field flow.

In recent years, theoretical studies of inviscid transonic flows have been largely carried out as part of more general problems of *boundary layer stability* (Bogdanov *et al.* 2010) and *boundary layer separation* (Ruban & Turkyilmaz 2000; Buldakov & Ruban 2002; Ruban *et al.* 2006). All these works focus on applying various asymptotic limits to the Navier–Stokes equations, resulting in triple-deck structures with an inviscid transonic flow in the upper tear. While the boundary layer stability problem leads to unsteady transonic equations, the problem of boundary layer separation due to various surface

irregularities is steady, and the relevant transonic flow in the upper tear can be studied extensively using the phase portrait and the hodograph method. This approach allowed Ruban & Turkyilmaz (2000) to discover a simple analytical solution which describes transonic flow with a free streamline emerging from a convex corner. Subsequently, Buldakov & Ruban (2002) used the analytical methods along with computations to study inviscid transonic flow in the vicinity of the sonic point on a smooth surface, and Ruban *et al.* (2006) studied transonic Prandtl-Meyer flow generated near a higher-order irregularity in the shape of body contour (such that the surface slope is regular, but wall curvature has a singularity).

All of the above mentioned works revealed that transonic *viscous-inviscid interaction*, a central mechanism in boundary layer separation, is different from the relevant sub- and supersonic cases. It appears that transonic separation gains its unique features not just through the upper tier of the triple deck where the non-linear Karman–Guderley equations replace the simple subsonic and supersonic interactive laws; more importantly, the inviscid transonic flow upstream of the interaction region proves to be capable of producing strong variations in the internal structure of the boundary layer approaching the triple deck (such variations can be referred to as the *cumulative effects*). The latter might cause drastic changes in the physical background on which the interaction between the boundary layer and the outer inviscid flow develops, leading to fundamentally different mechanisms of separation as compared to similar sub- and supersonic cases (for an overview of these differences see Yumashev 2010).

It has long been observed that various irregularities in the shape of a body contour can lead to viscous-inviscid interaction and, in certain cases, to boundary layer separation. The most obvious surface irregularities that can cause boundary layer separation are *corner points* and *humps*. Extensive studies show that the nature of the interaction process always appears to be predetermined by the exact type of the surface irregularity (for references see Sychev *et al.* 1998). In this respect it is worth comparing the effect of a *discontinuity in wall curvature* on subsonic, transonic and supersonic flows. While the more familiar corner points are known to cause separation at all speeds (Neiland 1974; Ruban 1974; Ruban & Turkyilmaz 2000), does the curvature break have similar effects? The analysis performed by Messiter & Hu (1975) shows that certain types of curvature discontinuity (with a flat wall upstream of the break) do not lead to separation at sub- and supersonic speeds. However, when the flow near a discontinuity in wall curvature is transonic, the situation may change significantly.

Because of the well known hierarchical strategy applied to high Reynolds number flows in the classical boundary layer theory, one first of all has to consider an inviscid transonic flow in a small vicinity of the curvature break. And even though the analysis of an inviscid flow is often treated only as a step towards the study of the boundary layer separation, it has an importance of its own. The local analysis reveals a complicated flow pattern depending on the ratio of the curvatures before and after the break. It is assumed that the *sonic point* coincides with the curvature discontinuity (§ 2), to ensure that the flow around it is transonic, and that the separation is local (i.e., the separation zone is confined within the small interaction region around the curvature break, as opposed to the global separation characterized by a free streamline with a semi-infinite separation zone behind it). This allows to work with local self-similar expansions.

In § 4 we develop a new technique of solving the Karman-Guderley equation in the ODE form numerically. The computational results are interpreted using the phase portrait technique introduced in § 3. In § 5 a complete theoretical explanation of the observed flow regimes is given based on the hodograph method.

The wall curvature discontinuity leads to the singular pressure gradients $\partial p/\partial x \sim$

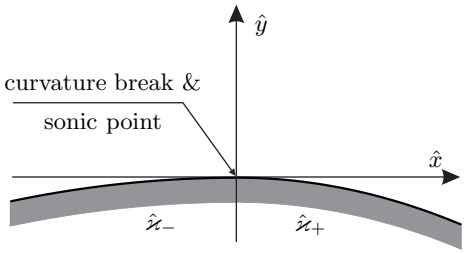


FIGURE 1. A discontinuity in wall curvature.

$G_\mp\,(\mp x)^{-1/3}$ upstream and downstream of the break, respectively (§ 2). This type of the singular pressure gradient is due to both the curvature break and the sonic point, and not just to the sonic point as suggested previously by Buldakov & Ruban (2002). It turns out to be possible to express the amplitude coefficients $G_\mp$ as implicit functions of the ratio of the curvatures (§ 5). This is a very significant result, especially in view of the subsequent study of the boundary layer separation caused by the singular pressure gradients.

One of the central concepts of transonic aerodynamics is the *limiting characteristic*. It corresponds to the singularity in the Karman-Guderley equation and appears to be an important boundary between physically different regions of transonic flow with respect to a propagation of small perturbations (see for example Liepmann & Roshko 1957; Landau & Lifshitz 1959; Cole & Cook 1986). Thanks to this property, certain low-speed supersonic flows which have not passed through the limiting characteristic yet can actually be decelerated to subsonic speeds without forming a *shock wave*. However, once a flow has passed through the limiting characteristic, it can only be decelerated to subsonic speeds by going though a shock. Due to the breadth and significance of this problem, we found it necessary to split the analysis of the flow regimes based on the hodograph method into two parts. In the present paper (Part 1) we only cover the flows that do not pass through the limiting characteristic and give theoretical explanation to the relevant numerical results (§ 5). In the following paper (Part 2) we apply the combination of the hodograph method and the phase portrait technique to extend analytical solutions beyond the limiting characteristic, prove that passing through the limiting characteristic inevitably leads to shock formation, and obtain a complete description of the flow behind the shock (including flow regimes with concave downstream wall).

To sum up, this study as a whole provides a detailed explanation of all possible transonic flow regimes depending on the ratio of the curvatures, most importantly the ones that pass through the limiting characteristic and consequently develop a weak shock.† It will be demonstrated in Part 2 that for such regimes the pressure amplitudes $G_\mp$ have multiple solutions (each with two distinct branches for a weak and a strong shock), suggesting that the local flow with a shock gains an extra degree of freedom and becomes dependent on the global flow. This is because small perturbations ("information") cannot propagate upstream once the flow passes through the limiting characteristic (§ 3).

## 2. Problem formulation

### 2.1. *Governing equations and boundary conditions*

Consider a 2D inviscid transonic flow of a perfect gas near a point of a discontinuity in wall curvature, Figure 1. The local surface shape close to a curvature break may be expressed as

$$\hat{y}_w(\hat{x}) = -\frac{\hat{\varkappa}_\pm \hat{x}^2}{2} + \dots, \qquad \hat{x} \gtrless 0\,,$$

where the hat denotes dimensional variables, $\hat{\varkappa}_\pm$ stand for the wall curvatures, and the dots represent higher-order terms in the coordinate expansions. In our definition $\hat{\varkappa}_\pm > 0$ for convex walls. The Cartesian coordinates $\hat{x}$, $\hat{y}$ can be scaled using either of the curvature radii $\hat{\varkappa}_\pm^{-1}$. If we take $L = \hat{\varkappa}_-^{-1}$ as a scale, the body surface will be given by

$$y_w(x) = \begin{cases} -\frac{x^2}{2}\,, & x < 0 \\ -\left(\frac{\hat{\varkappa}_+}{\hat{\varkappa}_-}\right)\frac{x^2}{2}\,, & x > 0 \end{cases}$$

in the scaled variables, showing that the local behaviour of the flow is likely to depend only upon the curvatures ratio $\hat{\varkappa}_+/\hat{\varkappa}_-$. However, the scale is not going to be specified since the local inviscid problem considered in this paper is invariant with respect to rescaling of spatial coordinates.‡ Furthermore, the scaled curvatures $\varkappa_\pm = L\,\hat{\varkappa}_\pm$ will be used henceforth, because they provide the same ratio.

To make sure the flow near the curvature discontinuity is transonic, let us assume that the point $(x, y) = (0, 0)$ where the curvature breaks is also a *sonic point*. The velocity at this point is equal to the local speed of sound $\hat{a}_*$, and it will be used for scaling the velocity components. Should the sonic point move towards either side of the curvature break, this would imply that the flow around the break has either subsonic or supersonic features, and a boundary layer separation is unlikely to happen (Messiter & Hu 1975).

By assuming that the oncoming flow is isoenthalpic, the Euler equations can be reduced to the system containing only the velocity components $U$, $V$ and the local speed of sound $a$:

$$\left.\begin{aligned} &\left(a^2 - U^2\right)\frac{\partial U}{\partial x} + \left(a^2 - V^2\right)\frac{\partial V}{\partial y} = UV\left(\frac{\partial U}{\partial y} + \frac{\partial V}{\partial x}\right)\,, \\ &\frac{U^2 + V^2}{2} + \frac{a^2}{\gamma - 1} = \frac{\gamma + 1}{2(\gamma - 1)}\,, \end{aligned}\right\} \tag{2.1}$$

where $\gamma$ is the specific heat ratio.¶ We are going to restrict the analysis to potential flows only, for which the velocity components may be expressed through the potential function $\Phi(x, y)$.

System (2.1) is solved subject to the impermeability boundary condition upstream and downstream of the curvature discontinuity:

$$V/U\big|_{y=y_w} = dy_w/dx = -\varkappa_\pm\, x\,, \qquad x \gtrless 0\,. \tag{2.2}$$

The downstream condition is written in the assumption that the separation zone is local, being confined within the interaction region.

† Even though a similar kind of a transonic flow was originally studied numerically by Buldakov & Ruban (2002), their work was mostly concerned with the regimes without a shock and did not deal with curvature discontinuity.

‡ The problem of the viscous-inviscid interaction, discussed in a separate paper, depends on the spatial scale through the definition of the Reynolds number.

¶ System (2.1) is written using the dimensionless variables.

### 2.2. *Asymptotic expansions for local self-similar solutions*

Boundary condition (2.2) may be transferred to the $y = 0$ axis in the leading order, providing $|\varkappa_\pm x| \ll 1$:

$$V|_{y=0,\, x\gtrless 0} = -\varkappa_\pm x\,. \tag{2.3}$$

This automatically restricts our attention to the upper half-plane, $y \geqslant 0$. As we move closer to the origin, no length scale can be assigned to the problem and the Euler equations are expected to admit self-similar solutions (Cole & Cook 1986); the scaled coordinates $(x, y)$ can be used as small parameters to construct asymptotic expansions in this local region. The intention to consider local behaviour of the inviscid flow is based on the knowledge that typical flow separation phenomena are also local (Sychev *et al.* 1998).

Introducing the similarity variable $\xi = x/y^\alpha$, where $\alpha$ is an unknown parameter which is to be determined, we construct asymptotic expansion of the velocity potential near the sonic point:

$$\Phi(x, y) = x + y^\sigma F(\xi)/(\gamma + 1) + \dots\,, \qquad \sigma = \sigma(\alpha)\,, \quad y \to 0\,, \quad \xi = O(1)\,. \tag{2.4}$$

The first term here corresponds to the main unperturbed flow with $U = 1$, $V = 0$ at the sonic point, whereas the second term represents the leading-order perturbation, with the function $F(\xi)$ being an order one quantity for $\xi = O(1)$. Substituting this expansion into (2.1) and using the principle of least degeneration results in the ODE (Frankl 1947):

$$\big[(\alpha\xi)^2 - F'\big]F'' - 5\alpha(\alpha - 1)\,\xi F' + 3(3\alpha - 2)(\alpha - 1)\,F = 0\,, \tag{2.5}$$

and shows that $\sigma = 3\alpha - 2$. Expression (2.4) is an asymptotic expansion for $y \to 0$ as long as $\alpha > 1$ and, consequently, $\sigma > 1$. A more strict argument leading to the introduction of the similarity variable $\xi = x/y^\alpha$ and the relevant asymptotic form (2.4) is based on *group theory* (Cole & Cook 1986).

Equation (2.5) is non-linear and has a singular point where $(\alpha\xi)^2 - F'$ turns zero. The singular point corresponds to the so-called *limiting characteristic* in the flow (Guderley 1957); upon passing through this characteristic, the flow becomes significantly supersonic and cannot be decelerated without a shock formation. It is well known that the limiting characteristic is different from the sonic line on which the local Mach number $\mathrm{M} = 1$ (Cole & Cook 1986). In this paper we are going to demonstrate that a formally supersonic flow which has already passed through the sonic line but has not yet reached the limiting characteristic may still be decelerated without a shock to become subsonic (section 5.6).

Since $y = 0$ corresponds to $\xi = \pm\infty$ depending on the sign of $x$, boundary condition (2.3) reduces to

$$\alpha\big[\lambda F - \xi F'\big]\big|_{\xi\to\pm\infty} \sim -(\gamma + 1)\varkappa_\pm\; x\, y^{3-3\alpha}\big|_{y\to 0}\,, \qquad x \gtrless 0\,, \tag{2.6}$$

where $\lambda = \frac{\sigma}{\alpha} = 3 - \frac{2}{\alpha}$. It is easily seen from (2.6) that $\alpha$ has to satisfy the constraint $3\alpha - 3 = \alpha$, yielding $\alpha = 3/2$, $\lambda = 5/3$. Hence, (2.6) takes the form

$$\lim_{\xi\to\pm\infty}\left[\frac{\lambda F}{\xi} - F'\right] = -\frac{(\gamma + 1)\varkappa_\pm}{\alpha}\,, \qquad x \gtrless 0\,. \tag{2.7}$$

The boundary-value problem (2.5), (2.7) can be studied both numerically and analytically.

One of the goals of this work is to find pressure gradients on both upstream and downstream walls as functions of the curvatures ratio. The wall pressure gradients are closely related to the asymptotic behaviour of $F(\xi)$ at $\xi \to \pm\infty$; equation (2.5) yields

$$F(\xi) = C_\pm(\pm\xi)^{3-\frac{2}{\alpha}} + D_\pm(\pm\xi)^{3-\frac{3}{\alpha}} + O\Big((\pm\xi)^{3-\frac{4}{\alpha}}\Big)\,, \qquad \xi \to \pm\infty\,,$$

where $C_\pm$ and $D_\pm$ are constants. Since $\alpha = 3/2$, the general expression takes the form

$$F(\xi) = C_\pm(\pm\xi)^\lambda \pm D_\pm\xi + \dots, \qquad \xi \to \pm\infty, \quad \lambda = \frac{5}{3}. \tag{2.8}$$

Substituting this into (2.7), we get

$$D_\pm = \mp(\gamma+1)\varkappa_\pm,$$

which means that the second term of the asymptotic form (2.8) is related to the impermeability condition on the wall. The first term, on the other hand, describes the pressure distribution on the wall. Indeed, the scaled pressure perturbation $p = (\hat{p} - \hat{p}_*)/\hat{\rho}_*\hat{a}_*^2$ can be expressed in terms of $F(\xi)$ using the Bernoulli equation:

$$p = -y^{2(\alpha-1)}F' + \dots; \tag{2.9}$$

$\hat{p}_*$ and $\hat{\rho}_*$ stand for the pressure and the density at the sonic point. Plugging (2.8) into (2.9) and setting $y = 0$ yields:

$$\left.\frac{\partial p}{\partial x}\right|_{\xi\to\pm\infty} = -C_\pm\frac{2\lambda(\alpha-1)}{\alpha}(\pm x)^{1-\frac{2}{\alpha}}, \qquad x \gtrless 0.$$

For the case of $\alpha = 3/2$ the gradient develops a singular behaviour of $(\pm x)^{-1/3}$ as long as $C_\pm \neq 0$, and so we need to find the relationship between $C_\pm$ and $\varkappa_+/\varkappa_-$.

The leading-order velocity perturbations $u$, $v$ are given by

$$\left.\begin{aligned} u &= (\gamma+1)(U-1) = (\gamma+1)(\partial\Phi/\partial x - 1) = y^{2\alpha-2}F'(\xi) \sim -p, \\ v &= (\gamma+1)V = (\gamma+1)\partial\Phi/\partial y = y^{3\alpha-3}\big[(3\alpha-2)F - \alpha\xi F'\big], \end{aligned}\right\} \tag{2.10}$$

while the local Mach number

$$\mathrm{M} = \frac{\sqrt{U^2+V^2}}{a} = 1 + \frac{1}{2}y^{2(\alpha-1)}F' + \dots. \tag{2.11}$$

## 3. Phase portrait

Let us now give an overview of the concept of the *phase portrait*, widely used in the theory of transonic flows (Guderley 1957; Cole & Cook 1986). This methodology is central for our study, and therefore we find it necessary to cover it in this paper briefly.

### 3.1. *Invariant transformations*

It is easy to notice that equation (2.5) admits the invariant group transformation

$$\xi = A\overline{\xi}, \qquad F = A^3\overline{F}, \tag{3.1}$$

where $A > 0$ is a stretch coefficient, and the bar denotes transformed variables. This is equivalent to the coordinate and curvature transformation

$$x = B\overline{x}, \quad y = B\overline{y}, \qquad \varkappa_\pm = B^{-1}\overline{\varkappa}_\pm, \quad B = A^{\frac{1}{1-\alpha}}. \tag{3.2}$$

Boundary conditions (2.7) are also invariant with respect to the transformation when $\alpha = 3/2$ (Yumashev 2010).

In order to make the solution independent on a choice of the group constant $A$, we shall introduce two new functions of $\xi$ proportional to the velocity perturbations $u$, $v$

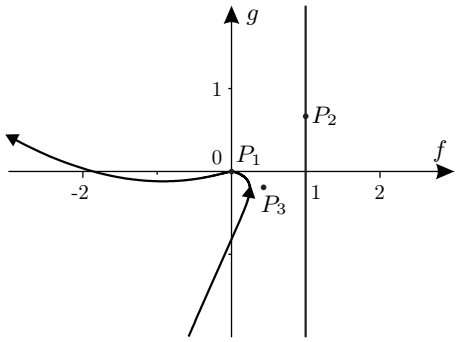


FIGURE 2. A typical phase trajectory in the $(f, g)$ plane, with $P_1$, $P_2$ and $P_3$ being the stationary points of equations (3.5).

(Guderley 1957): †

$$f(\xi) = \frac{F'}{\alpha^2\xi^2} \equiv \frac{(u/y)}{\alpha^2\xi^2}\,, \quad g(\xi) = \frac{\lambda F - \xi F'}{\alpha^2\xi^3} \equiv \frac{(v/x)}{\alpha^3\xi^2}\,. \tag{3.3a, b}$$

Introducing a new independent variable $\chi$ through

$$d\chi = \frac{d\xi}{(f-1)\alpha\xi}\,, \tag{3.4}$$

one can easily convert equation (2.5) to the following non-singular autonomous system (Guderley 1957):

$$\left.\begin{aligned} df/d\chi &= 2f + 3(\alpha-1)g - 2\alpha f^2\,, \\ dg/d\chi &= 3g + 2(\alpha-1)f^2 - 3\alpha f g\,. \end{aligned}\right\} \tag{3.5}$$

Now each solution of equation (2.5) may be treated as a phase trajectory in the $(f, g)$ plane, as shown in Figure 2. Each such trajectory represents a family of solutions for all possible values of $A$, i.e. is invariant with respect to coordinate transformation (3.2), and runs in a certain direction as $\xi$ is changing from $-\infty$ to $\infty$. However, few difficulties arise immediately.

First of all, transformation (3.4) of the independent variable has two singular points $\xi = 0$, $f = 1$, and passing through either of them alters the direction of changing of $\chi$ with respect to the old variable $\xi$. Hence, the phase plane should have several sheets, with different parts of the trajectory running on different sheets according to (3.4).‡ Since $F(0) \neq 0$, $F'(0) \neq 0$ in most of the cases, typical phase trajectories stretch to infinity when $\xi \to 0$ and, in addition to moving onto a new sheet of the phase plane, undergo reflection in the $g = 0$ axis as $\xi$ changes sign (see (3.3)).

The line $f = 1$ needs a particular attention. It corresponds to the singular point $F' = \alpha^2\xi^2$ of equation (2.5), and therefore will be called the *singular line*. It turns out that the phase trajectories are only able to pass through the singular line at the point with coordinates $(f, g) = \left(1, \frac{2}{3}\right)$; the relevant value $\xi_c$ of variable $\xi$ defines the so-called *limiting characteristic* in the physical plane. This characteristic is important because it forms a boundary between two physically different regions.

Equations (3.5) are strongly non-linear and cannot be integrated analytically for the case of $\alpha = 3/2$; in this formulation the problem may only be solved numerically. Never-

† Defined in (2.10), $u$ and $v$ are also invariant with respect to transformation (3.2).

‡ We are going to plot all the fragments of a single curve (running on different sheets) on the same graph.

theless, analyzing *stationary points* of system (3.5) provides an insight regarding several important properties of the transonic flow (Cole & Cook 1986).

### 3.2. *Stationary points of the phase portrait equations*

Equations (3.5) have three stationary points, where the right-hand sides simultaneously become equal to zero (Guderley 1957). They are $P_1 = (0,0)$, $P_2 = \left(1, \frac{2}{3}\right)$ and $P_3 = \left(\frac{1}{\alpha^2}, -\frac{2}{3\alpha^3}\right)$, as shown in Figure 2.†

**1.** $P_1 = (0,0)$ is a node with half lines $g = 0$ and $g = \frac{1}{3(\alpha-1)} f$ (the latter becomes $g = \frac{2}{3} f$ when $\alpha = 3/2$). The linearised system has a pair of positive eigenvalues $\lambda_1 = 2$ and $\lambda_2 = 3$, yielding the local solution $f = C\,|g|^{2/3} + 3(\alpha-1)g$ for the phase trajectories, $C = \text{const}$. Being the origin in the phase plane, point $P_1$ corresponds to both the upstream and downstream walls. Therefore, the trajectories start from the origin when $\xi = -\infty$ and return to it when $\xi = \infty$. Depending on the sign of $f$, the flow in the vicinity of the wall can be either subsonic or supersonic. In the limiting cases $C = \infty$ and $C = 0$ the trajectories follow the first and the second half line, respectively. In all other cases $f \sim |g|^{2/3}$ in the leading order, which means that specifying the first two terms of the asymptotic form (2.8) is equivalent to setting the constant

$$C = \lim_{\xi \to \pm\infty} f\,|g|^{-2/3}\,.$$

This result will be used in section 5.3 to obtain boundary conditions in the hodograph plane.

**2.** $P_2 = \left(1, \frac{2}{3}\right)$ is a node located on the singular line, with half lines $g - \frac{2}{3} = f - 1$ and $g - \frac{2}{3} = \mu\,(f-1)$, where $\mu = \frac{2(2-\alpha)}{3(\alpha-1)}$ ($\mu = 2/3$ for $\alpha = 3/2$). The linearized system has a pair of negative eigenvalues $\lambda_1 = -(\alpha+1)$, $\lambda_2 = -6(\alpha-1)$, and the relevant local solution can be found in Cole & Cook (1986). The presence of the node $P_2$ on the singular line leads to important consequences. It appears that the coordinate line $\xi = \xi_c$ in the physical plane, with $\xi_c$ being the common root of the equations $f(\xi_c) = 1$, $g(\xi_c) = \frac{2}{3}$, coincides with a characteristic of the Euler equations. One also needs to make sure that on those coordinate lines which coincide geometrically with the characteristics the so-called *compatibility condition* holds.‡ Upon substituting the expansions for the velocity components into the compatibility condition and setting $f = 1$, it yields $g = 2/3$ in the leading order, thus proving that the only place where the phase trajectories can pass through the singular line is $P_2$ (Ruban & Turkyilmaz 2000).

There appears to be a fundamental connection between the limiting characteristic and the way small perturbations propagate in transonic flows (Yumashev 2010). When $\xi < 0$, the coordinate lines have a negative slope and can coincide with the characteristics of the second family; the latter bring information from the outer flow to the wall. Now, if $f < 1$, i.e. the phase trajectory has not yet passed to the right of the singular line, the characteristics are steeper than the coordinate lines and the normal component of velocity on these lines is smaller than the local speed of sound. On the contrary, if $f > 1$, then the characteristics are flatter than the coordinate lines, and the normal component of velocity on these lines is greater than the local speed of sound. Consequently, small perturbations from the downstream regions do not penetrate through the coordinate lines in the upstream direction. It means that if a transonic flow passes through the limiting characteristic (i.e., the phase trajectories tunnel to the right of the singular line

† We are not specifying the value of $\alpha$ for the sake of generality.

‡ This is the necessary condition for a solution to exist along the characteristics, and it imposes a certain restriction on the velocity components, leading to the introduction of the *Riemann invariants* (Liepmann & Roshko 1957).

through the point $P_2$), the downstream regions do not affect the flow upstream. In the subsequent paper (Part 2) we shall demonstrate that this property provides one extra degree of freedom in the local solution, requiring to specify one parameter from the global flow in order to describe the local flow uniquely.

When $\xi > 0$, the above results hold for the characteristics of the first family (with a positive slope) transferring information from the wall to the outside flow. It will be shown in Part 2 that for our particular problem $\xi_c < 0$; the value of $\xi_c$ will be obtained analytically.

**3.** $P_3 = \left(\frac{1}{\alpha^2}, -\frac{2}{3\alpha^3}\right)$ is a saddle point with the half-lines directed along the vectors

$$\left\|1\,,\,\tfrac{2(2\alpha-1)}{3\alpha(\alpha-1)}\right\|^T\,, \qquad \left\|1\,,\,-\tfrac{1}{\alpha}\right\|^T\,.$$

The linearised system has eigenvalues $\lambda_1 = -\frac{\alpha+1}{\alpha}$, $\lambda_2 = \frac{6(\alpha-1)}{\alpha}$ with opposite signs. When the phase trajectories approach the saddle point, their direction undergoes an abrupt change. This affects the physics of the flows by providing a border between the trajectories corresponding to different flow regimes. The saddle point creates an obstacle for those trajectories that move towards the singular line in the lower half-plane $g < 0$ (Figure 2), and makes them turn either towards the subsonic region, or towards the point $P_2$ where an intersection with the singular line is allowed. In some special cases the trajectories find themselves moving along the saddle point half-lines (Yumashev 2010).

## 4. Numerical solutions of the Karman-Guderley equation

To find the pressure gradients on both walls for a given ratio of the curvatures, we need to obtain the phase trajectories for all $\xi \in (-\infty, \infty)$. The only way to do that, as long as equation (2.5) or system (3.5) are being considered, is to solve the relevant boundary-value problem numerically.

### 4.1. *Transformation of the variables*

To increase the accuracy of numerical results, let us introduce a simple transformation of the variable $\xi$ and the function $F(\xi)$ that allows to work with a finite computational domain and simpler boundary conditions. According to the asymptotic behaviour (2.8) of $F(\xi)$ at $\xi \to \pm\infty$, one can define a new function $G(s)$:

$$F(\xi) = \left[(\gamma+1)\varkappa_-\right]^{1/\alpha} \operatorname{sign}(\xi)\,|\xi|^{\lambda}\,G(s)\,, \tag{4.1$a$}$$

with the new independent variable $s$ given by

$$\xi = \left[(\gamma+1)\varkappa_-\right]^{\alpha-1} \operatorname{sign}(s)\left(\tan|s|\right)^{\alpha} \tag{4.1$b$}$$

on the finite domain $-\frac{\pi}{2} \leqslant s \leqslant \frac{\pi}{2}$. The $|\xi|^{\lambda}$ term is used in (4.1$a$) to make $G(s)$ finite when $s = \pm\frac{\pi}{2}$, and taking $\tan|s|$ to the power of $\alpha$ in (4.1$b$) ensures that $dG/ds$ is also finite. Both $s$ and $G(s)$ are invariant with respect to re-scaling (3.1), thanks to the terms with $\varkappa_-$ in the above equations.

Transformation (4.1$b$) monotonously maps the infinite region $-\infty < \xi < \infty$ into the domain $-\frac{\pi}{2} < s < \frac{\pi}{2}$ which is more suitable for computations. The limiting values of $G(s)$, defined as

$$G_{\pm} = \mp\, G(\pm\pi/2)\,,$$

are directly related to the pressure gradients on the walls:

$$\left.\frac{\partial p}{\partial x}\right|_{y=0,\,x\gtrless 0} = G_{\pm}\left[(\gamma+1)\varkappa_-\right]^{1/\alpha}\frac{2\lambda(\alpha-1)}{\alpha}\,(\pm\,x)^{1-\frac{2}{\alpha}} + \ldots\,, \qquad |x| \ll 1\,. \tag{4.2}$$

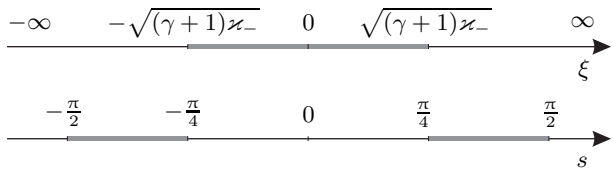


FIGURE 3. Computational domains for $\xi$ and $s$.

This is reduced to

$$\left.\frac{\partial p}{\partial x}\right|_{y=0,\,x\gtrless 0} = \mp\, k\, G_{\pm}\,(\pm\, x)^{-1/3} + \ldots\,, \qquad k = \frac{10\big[(\gamma+1)\varkappa_-\big]^{2/3}}{9} \tag{4.3}$$

when $\alpha = 3/2$, thus yielding the $(\pm\, x)^{-1/3}$ singularity in the pressure gradients.

Transformations (4.1$a$)–(4.1$b$) result in the simple boundary conditions for $G(s)$:

$$\left.\frac{dG}{ds}\right|_{s=\pm\frac{\pi}{2}} = \begin{cases} \frac{\varkappa_+}{\varkappa_-}\,, & x>0\,, \\ -1\,, & x<0\,, \end{cases} \tag{4.4$a$}$$

and the equation for $G(s)$ is

$$\begin{aligned} &\sin^2 s\,\frac{d}{ds}\left(\sin^2 s\,\frac{dG}{ds}\right) = \left(\lambda G + \frac{\sin(2s)}{2\alpha}\,\frac{dG}{ds}\right) \\ &\times\left[\lambda(\lambda-1)G + \frac{\lambda\sin(2s)}{2\alpha}\,\frac{dG}{ds} + \frac{\cos^2 s}{\alpha^2}\,\frac{d}{ds}\left(\sin^2 s\,\frac{dG}{ds}\right)\right]. \end{aligned} \tag{4.4$b$}$$

The solution of the boundary-value problem (4.4$a$)–(4.4$b$) obviously depends only on the ratio of the curvatures. Since the problem does not contain the specific heat ratio $\gamma$, it means that physical pressure gradients, according to (4.3), are related to $\gamma$ via the factor $(\gamma+1)^{2/3}$.

Equation (4.4$b$) can be integrated numerically for any $s \neq 0$; however, the solution develops a singularity, namely $G(s) \sim |s|^{-\alpha\lambda}$, as $|s| \to 0$. Thus, original equation (2.5) has to be solved in the vicinity of $\xi = 0$, and the corresponding solution should be matched with $G(s)$ on both sides of $\xi = 0$. By restricting the domain for $s$ (where equation (4.4$b$) is solved) to $-\frac{\pi}{2} < s < -\frac{\pi}{4}$ and $\frac{\pi}{4} < s < \frac{\pi}{2}$, we get the relevant domain for $\xi$ (where equation (2.5) is solved):

$$-\sqrt{(\gamma+1)\varkappa_-} < \xi < \sqrt{(\gamma+1)\varkappa_-}\,,$$

as shown in Figure 3. At the joints, one needs to match $F(\xi)$ with $G(s)$ using (4.1$a$), and $dF/d\xi$ with $dG/ds$ via

$$\left.\frac{dF}{d\xi}\right|_{\xi=\pm\sqrt{(\gamma+1)\varkappa_-}} = \pm\,(\gamma+1)\varkappa_-\,\tan s\left[\lambda G + \frac{\sin(2s)}{2\alpha}\,\frac{dG}{ds}\right]\Bigg|_{s=\pm\frac{\pi}{4}}.$$

In order to reconstruct the phase trajectories, we use original definition (3.3) within the computational domain for $\xi$, whereas in the domain of the transformed variables $s$, $G(s)$ equations

$$f(s) = \frac{1}{\alpha^2\tan^2 s}\left[\lambda G + \frac{\sin(2s)}{2\alpha}\,\frac{dG}{ds}\right], \quad g(s) = -\frac{\sin(2s)}{2\alpha^3\tan^2 s}\,\frac{dG}{ds} \tag{4.5}$$

are employed.

Finally, for those trajectories that happen to pass through the point $P_2$ both equations

(2.5) and (4.4$b$) fail, as the coefficient in front of the second derivative becomes zero. Therefore, on approaching $P_2$ we are going to solve the equation

$$\frac{dg}{df} = \frac{3g + 2(\alpha - 1)f^2 - 3\alpha f g}{2f + 3(\alpha - 1)g - 2\alpha f^2}\,, \tag{4.6}$$

obtained from (3.5) and written directly for the phase variables. In the point $P_2$ itself both the numerator and the denominator in (4.6) are equal to zero, but their ratio is finite and is equal to 1 when $\alpha = 3/2$. This is used to eliminate the singularity in (4.6) and pass through the critical point $P_2$.

### 4.2. *Numerical results for the phase portrait and the pressure gradients*

Instead of dealing with the original boundary-value problem which arises when both curvatures are specified, one can consider a different physical situation. Let us assume that we know both the curvature and the pressure gradient on the upstream wall, while the downstream curvature and pressure gradient are unknown. From (4.2) it follows that specifying the upstream pressure gradient is equivalent to setting the value of $G_-$, and along with the upstream condition (4.4$a$) for $dG/ds$ this defines the initial-value problem for $G(s)$, which can be solved numerically using marching with a second-order scheme. Integrating equations (4.4$b$), (2.5) within the domains defined in section 4.1 (Figure 3), we calculate the phase variables $f$, $g$ and plot the relevant phase trajectory along the way. Once the final point $s = \pi/2$ is reached, we get the values of $G_+$, $dG/ds|_+$, and therefore can work out both the downstream pressure gradient and the curvatures ratio from equations (4.3), (4.4$a$); since $\varkappa_-$ is specified, the latter provides $\varkappa_+$.

Notice that for $\alpha = 3/2$ equation (2.5) admits a simple analytical solution

$$F(\xi) = -(\gamma + 1)\varkappa\,\xi\,, \qquad -\infty < \xi < \infty \tag{4.7}$$

where $\varkappa$ is an arbitrary constant. According to (4.1$a$), it yields $G_\pm = 0$, i.e. zero pressure gradients on both walls in the leading order. The perturbations of the velocity components, defined in (2.10), in this case are:

$$u = y\,F' = -(\gamma + 1)\varkappa\,y\,, \quad v = \alpha y^{3/2}\left[\lambda F - \xi F'\right] = -(\gamma + 1)\varkappa\,x\,. \tag{4.8}$$

Therefore, (4.7) describes a potential vortex flow outside a wall with a constant curvature $\varkappa = \varkappa_- = \varkappa_+$; for convex walls $\varkappa > 0$ and the flow in the vortex is subsonic. This solution can be used as a starting point for the calculations. The corresponding phase trajectory is simply a straight line $g = \frac{2}{3}f$, $f < 0$, starting from the origin when $\xi = -\infty$, then moving to ($f = -\infty$, $g = -\infty$) as $\xi \to 0$, and eventually returning back to the origin when $\xi \to \infty$ (Figure 4).† The $g = \frac{2}{3}f$ line also coincides with one of the half-lines of the stationary point $P_1$.

Based on the above results, we integrate the initial-value problem for a small negative value of $G_-$ (favourable pressure gradient on the upstream wall), calculating the phase trajectory and the downstream wall parameters. We then increase $|G_-|$ slightly (keeping $G_-$ negative) and solve the problem numerically again. By repeating the procedure, we obtain a family of the phase trajectories for negative values of $G_-$ (few of them are shown in Figure 4), and plot $\varkappa_+/\varkappa_-$ versus $G_-$ (Figure 5, left). Figure 4 suggests that when $G_- < 0$, the trajectories start into the subsonic half-plane ($f < 0$), i.e. the oncoming flow with a favourable pressure gradient is subsonic. After crossing the line $g = 0$ (where $v$ changes the sign), the trajectories head on to infinity as $\xi \to 0^-$, get reflected in the

† Note that the reflection rule, derived in section 3.1 for a typical trajectory when $\xi$ changes its sign, is not applicable in this case since $g$ appears to be an even function of $\xi$.

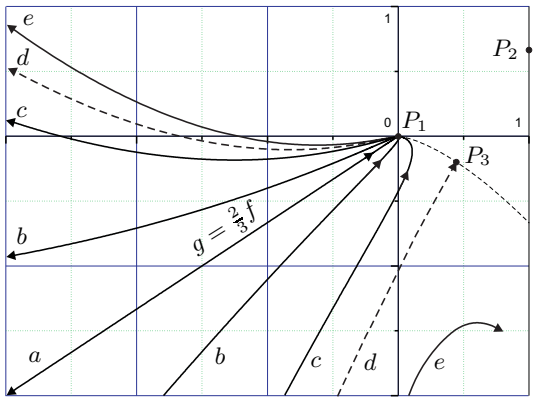


FIGURE 4. Numerical results for the phase trajectories corresponding to different ratios of the curvatures; $a$: $\frac{\varkappa_+}{\varkappa_-} = 1$; $b$ and $c$: $1 < \frac{\varkappa_+}{\varkappa_-} < \infty$; $d$: $\frac{\varkappa_+}{\varkappa_-} = \infty$; $e$: trajectories which cross the singular line in an illegitimate place and therefore have to be rejected.

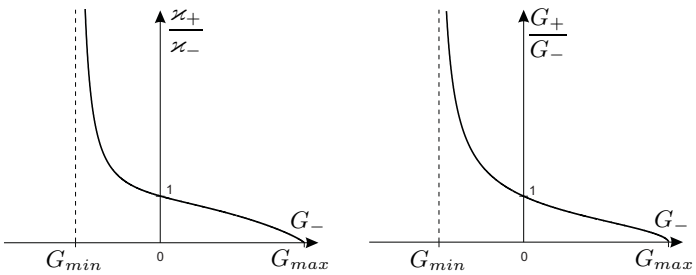


FIGURE 5. Numerical results for the ratio of the curvatures and the ratio of the gradients for different values of the upstream pressure gradient $G_-$.

$g = 0$ line, then enter the supersonic half-plane ($f > 0$) and finally return to the origin, thanks to the presence of the saddle point $P_3$. Thus, the flow becomes supersonic near the downstream wall. The larger $|G_-|$ is, the wider the trajectories go with respect to line $g = \frac{2}{3}f$, and their supersonic fragments come closer to the saddle point. As a result, for some $G_- = G_{min} < 0$ the trajectory ends at the saddle point.‡ The consequences of this kind of a behaviour have already been mentioned in section 3.2, and will be described in detail in section 5.7. Finally, when $|G_-|$ becomes greater that $|G_{min}|$, the trajectories turn to the right of the saddle point and approach the singular line, attempting to cross it at an illegitimate place (Figure 4). Hence, these solutions have to be rejected, which means that no favourable upstream pressure gradients stronger than $|G_{min}|$ can exist.

From Figure 5, left, we see that oncoming subsonic flows (which have $G_- < 0$) correspond to $\varkappa_+/\varkappa_- > 1$.† The ratio increases with $|G_-|$, leading to a flatter upstream wall for stronger favourable pressure gradients, and tends to $\infty$ when $G_- \to G_{min}^+$. This limit can correspond either to $\varkappa_+ \to \infty$, $\varkappa_- > 0$ or $\varkappa_- \to 0^+$, $\varkappa_+ > 0$, due to the problem's invariance with respect to re-scaling (3.2). In the first case the size of the region where the self-similar solutions are valid tends to zero;‡ however, for the observer who 'sits' in

‡ Analytical expression for $G_{min}$ will be obtained in section 5.5.

† Positive values of $G_-$ in Figure 5 correspond to a supersonic flow on the upstream wall which will be discussed later.

‡ Recall that transferring boundary condition (2.2) to the $y = 0$ axis is only possible when

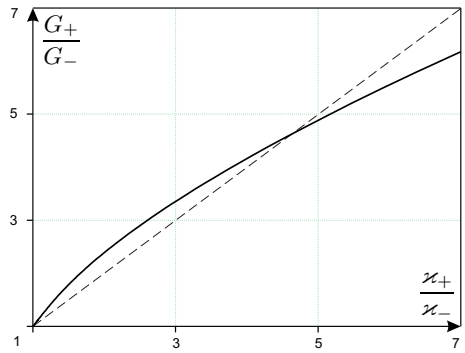


FIGURE 6. The ratio of the pressure gradients on the walls as a function of the ratio of the curvatures (plotted for the case of $\frac{\varkappa_+}{\varkappa_-} > 1$).

the self-similar region itself (small enough for the solutions to be valid) the upstream wall becomes a flat plate ($\varkappa_- \to 0$), whereas the downstream wall has $\varkappa_+ = O(1)$, thus corresponding to the second interpretation. By choosing

$$L = \left[\max(\hat{\varkappa}_-, \hat{\varkappa}_+)\right]^{-1}$$

as a scale, we can restrict dimensionless curvatures to $0 \leqslant \varkappa_\pm \leqslant 1$ to avoid the infinities and additional re-scaling.

The pressure gradients ratio $G_+/G_-$ is shown in Figure 5, right, as a function of $G_-$. As with the curvatures ratio, it is greater than 1 when $G_- < 0$, suggesting that the downstream pressure gradient is also favourable and is stronger than the upstream gradient. Both gradients vanish in the limit $\varkappa_+/\varkappa_- \to 1$ (no discontinuity in the curvature), although the gradients ratio tends to 1. In the opposite limit $\varkappa_+/\varkappa_- \to \infty$ the ratio also tends to infinity. Indeed, on a much flatter upstream wall the pressure gradient should be significantly smaller, i.e. $G_- \ll G_+$ and $G_+/G_- \to \infty$.

In Figure 6 the gradients ratio is plotted versus $\varkappa_+/\varkappa_-$.† When $\varkappa_+/\varkappa_-$ is increasing from 1, $G_+/G_-$ at first becomes slightly bigger than the curvatures ratio, but at $\varkappa_+/\varkappa_- \approx 4.7$ the situation changes to the opposite, ultimately leading to the following asymptotic behaviour:‡

$$\frac{G_+}{G_-} \sim \left(\frac{\varkappa_+}{\varkappa_-}\right)^{2/3}, \qquad \frac{\varkappa_+}{\varkappa_-} \to \infty\,.$$

Let us now move on to positive $G_-$ in the initial value problem; in this case the upstream pressure gradient is adverse (see (4.3)). By increasing $G_-$ slightly after each computation, we cover the whole range of possible values of adverse pressure gradients, plot the relevant phase trajectories and obtain the downstream wall parameters ($G_+$ and $\varkappa_+/\varkappa_-$). A selection of the trajectories is shown in Figure 7. This time they start into the supersonic half-plane $f > 0$ (i.e. the flow near the upstream wall is supersonic), but soon after that turn abruptly towards the subsonic half-plane, thanks to the presence of the saddle point. Despite the fact that the flow is originally supersonic, it does decelerate to subsonic speeds without a shock formation. In the subsequent sections we shall give

$|\varkappa_\pm x| \ll 1$, which means that the regions between the curved walls and the line $y = 0$ are negligible.

† This graph, unlike the previous one, is plotted for the case of a subsonic flow on the upstream wall only, i.e. for $\varkappa_+/\varkappa_- > 1$.

‡ This comes from the analysis of equations (5.28) in section 5.5.

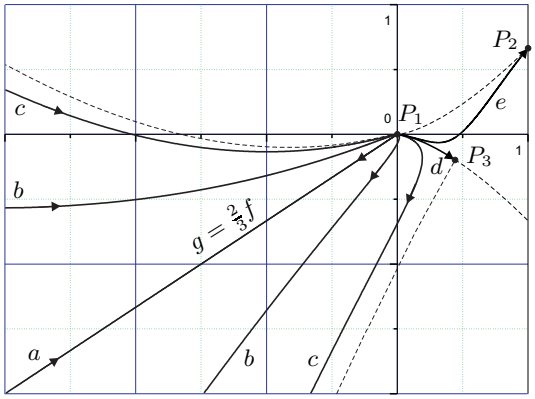


FIGURE 7. Numerical results for the phase trajectories corresponding to different ratios of the curvatures; $a$: $\frac{\varkappa_+}{\varkappa_-} = 1$; $b$, $c$: $0 < \frac{\varkappa_+}{\varkappa_-} < 1$; $d$: $\frac{\varkappa_+}{\varkappa_-} = 0$; $e$: trajectories which pass through the singular line via the only allowed point $P_2$. The dashed lines represent the limiting shape of the trajectories from the family $a$, $b$, $c$ when $\frac{\varkappa_+}{\varkappa_-} \to 0^+$, and the so-called *critical lines* in the supersonic half-plane (see section 5.2).

a rigorous proof that this is only possible when the phase trajectories remain on the left of the singular line.¶

After crossing the sonic line, the trajectories travel to ($f = -\infty$, $g = -\infty$), reflect in the $g = 0$ axis and return back to the origin (crossing line $g = 0$ on the way). Thus, the behaviour totally resembles the one of the trajectories in the previous regime (subsonic oncoming flows), with the only difference in the direction of travelling along the trajectories. Again, the larger the adverse pressure gradient on the upstream wall is, the wider the trajectories go with respect to $g = \frac{2}{3}f$. The relevant curvatures ratio is plotted versus $G_-$ in Figure 5, left. Now the ratio is within $(0, 1)$ and is diminishing with $G_-$; for some $G_- = G_{max} > 0$ it becomes zero, referring to either $\varkappa_+ \to 0^+$ or $\varkappa_- \to \infty$ (with the second curvature being an order-one quantity in both cases).† As $G_- \to G_{max}^-$, the trajectory approaches the saddle point $P_3$, and ends up in it when $G_- = G_{max}$. This time it reaches the saddle point when $\xi \to 0^-$ along the second linear asymptote (section 5.7).

The downstream pressure gradient $G_+$ is now also adverse (Figure 5, right). Overall, there appears to be a symmetry between the two regimes discussed above with respect to the transformation $x \longleftrightarrow -x$; in other words, physical processes in these flows are reversible. It is worth plotting both $G_-$ and $G_+$ as functions of the curvature's ratio (Figure 8). The two regimes discussed above have a similar property: knowing any pair of the physical parameters, for example $(\varkappa_-, \varkappa_+)$, or $(\varkappa_-, G_-)$, allows to determine the other two uniquely ($(G_-, G_+)$ or $(\varkappa_+, G_+)$ respectively). It means that by knowing, say, both of the curvatures (which is physically reasonable) one can work out the local flow regardless of the global flow, since no free parameters remain in the local solutions.

Finally, one has to say a few words on what happens when $G_-$ becomes larger that $G_{max}$. Recall that in the opposite case when $G_- < G_{min} < 0$ we had physically mean-

¶ Recall that in section 3.2 we argued that when $f < 1$, small perturbations may penetrate back through the coordinate lines, resulting in an influence of the downstream regions on the upstream ones (essential property of subsonic flows). Therefore, supersonic flows with $0 < f < 1$ are somewhat inferior and allow smooth deceleration.

† Note that $G_{max} \neq |G_{min}|$; analytical expression for $G_{max}$ will be given in section 5.6.

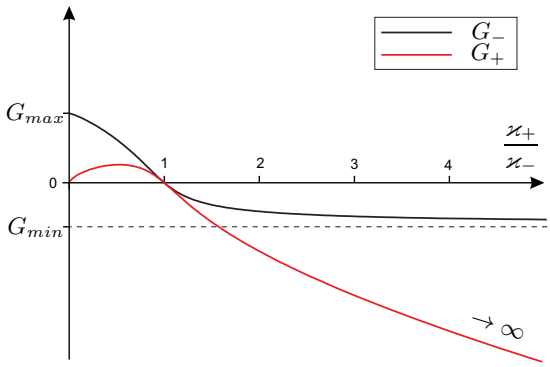


FIGURE 8. Upstream and downstream pressure gradients as functions of the ratio of the curvatures.

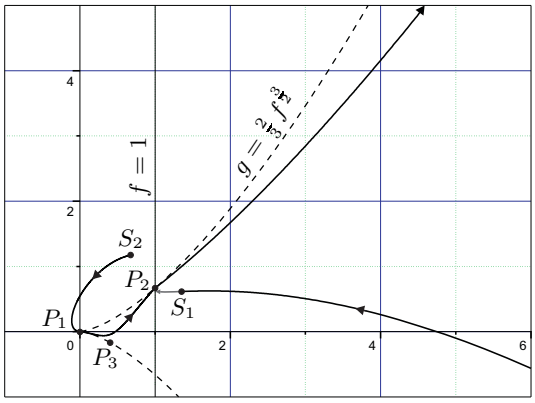


FIGURE 9. A typical phase trajectory which tunnels through the singular line.

ingless solutions with the trajectories trying to cross the singular line in an illegitimate place. However, for $G_- > G_{max}$ the trajectories go above the saddle point $P_3$; the latter makes them turn upwards and head on towards the node $P_2$ representing the limiting characteristic (Figure 7). This point provides the only possible passage through the singular line. Upon tunnelling through $P_2$, the trajectories travel further on the right of the singular line towards ($f = \infty$, $g = \infty$) (corresponding to $\xi \to 0^-$), are reflected in axis $g = 0$ and return back to the singular line, trying to cross it slightly below $P_2$ (Figure 9). Since this kind of a crossing is prohibited, the only way to return into the origin and satisfy the downstream boundary condition is to undergo a jump to the other side of the singular line. The jump would obviously correspond to a shock in the physical plane. A detailed analysis of such flows (which are irreversible due to the shock formation) is given in Part 2.‡

‡ Due to the fact that the flow passes through the limiting characteristic before developing the shock, it gains one extra degree of freedom (through the loss of a mutual interaction between the downstream and the upstream regions). In this case one needs to specify any three of the four main parameters ($\varkappa_\pm$, $G_\pm$) of the local flow to find the remaining one. This is totally different from the other flow regimes studied so far, and may be treated as a dependence of the local solution upon the global solution. Thus, along with both curvatures we now have to specify one of the pressure gradients in order to obtain a unique local flow pattern. Having one extra free

## 5. Hodograph method

In this section we are going to give a theoretical explanation of the numerical results obtained in § 4, describing all the possible transonic flow patterns near curvature break. However, the flow regimes that involve passing through the limiting characteristic will be discussed in a separate paper (Part 2).

### 5.1. *Direct and Inverse problems*

Our problem is two-dimensional, and so it admits a *momentum representation*, as opposed to the *coordinate representation* used in previous sections (Chaplygin 1902). This implies treating the perturbations $u$, $v$ of the velocity components as the independent variables, with the spatial coordinates being their functions: $x = x(u, v)$, $y = y(u, v)$. In the coordinate representation the flow in a small vicinity of the sonic point is described by the potential $\Phi(x, y) = x + \phi(x, y)/(\gamma + 1) + ...$, where $\phi(x, y)$ is a leading-order perturbation related to $u$, $v$ and $F(\xi)$ in the following way (see (2.10), (2.4)):

$$u = \frac{\partial \phi}{\partial x}\,, \quad v = \frac{\partial \phi}{\partial y}\,, \quad \phi(x, y) = y^{3\alpha-2} F(\xi)\,, \qquad y \to 0\,, \quad \xi = O(1)\,.$$

The functions $u$, $v$ satisfy the Karman–Guderley equations,

$$u\,\frac{\partial u}{\partial x} - \frac{\partial v}{\partial y} = 0\,, \quad \frac{\partial u}{\partial y} = \frac{\partial v}{\partial x}\,, \tag{5.1$a, b$}$$

which result from the Euler equations in the assumption of small transonic perturbations (Cole & Cook 1986). After inverting the roles of independent and dependent variables, equations (5.1) are transformed into the so-called Trikomi equations; these may be converted into a pair of linear second order equations for the functions $x(u, v)$ and $y(u, v)$ separately:

$$u\,\frac{\partial^2 y}{\partial v^2} - \frac{\partial^2 y}{\partial u^2} = 0\,, \quad u\,\frac{\partial^2 x}{\partial v^2} - \frac{\partial^2 x}{\partial u^2} + \frac{1}{u}\,\frac{\partial x}{\partial u} = 0\,. \tag{5.2$a, b$}$$

The transformation from system (5.1) to system (5.2) is possible when the Jacobian

$$J_{uv} = \left|\mathrm{Det}\begin{bmatrix} \partial x/\partial u & \partial y/\partial u \\ \partial x/\partial v & \partial y/\partial v \end{bmatrix}\right| \neq 0\,. \tag{5.3}$$

If $J_{uv} = 0$ for certain solutions of (5.2), the corresponding functions $u(x, y)$ and $v(x, y)$ are many-valued and these solutions have no physical meaning.† On the contrary, if $J_{uv} = \infty$ at some point, the functions $x(u, v)$, $y(u, v)$ are many-valued, suggesting that the same values of $u$, $v$ occur in several different places within the flow, which is a normal situation. However, in this case the original equations (5.1) have to be solved in order to avoid the difficulties in transforming $x(u, v)$, $y(u, v)$ to $u(x, y)$, $v(x, y)$.

From now on we shall call the problem described by system (5.1) with boundary conditions (2.2) the *direct problem* (coordinate representation), and the problem described by system (5.2) with the appropriate boundary conditions the *inverse problem* (momentum representation). The $(u, v)$ plane in which the inverse problem is being solved is known as the *hodograph plane* (Chaplygin 1902).

parameter results in a greater variety of regimes, for example flows over concave downstream walls with $\varkappa_+ < 0$.

† In fluid mechanics one expects to find a single pair of values of the velocity components $u$, $v$ at any given point $(x, y)$ unless there is a shock wave.

### 5.2. *Self-similar solutions of the Trikomi equations*

The inverse problem also admits a self-similar solution near the sonic point (in which the wall curvature breaks). Introducing the similarity variable $\zeta = u/v^{\beta}$, where $\beta$ is an unknown parameter, we represent $x(u,v)$ and $y(u,v)$ in the form

$$x(u,v) = v\,\psi(\zeta) + \dots\,, \quad y(u,v) = u\,\varphi(\zeta) + \dots\,, \tag{5.4$a$, $b$}$$

with the functions $\varphi(\zeta)$, $\psi(\zeta)$ being of the same nature as $F(\xi)$ in the direct problem.† The quasi-linear structure of these dependencies follows from the fact that $v$ is linear with respect to $x$ according to boundary condition (2.2), and also from the fact that in the limiting case $\varkappa_- = \varkappa_+ = \varkappa$ the direct problem admits the simple solution

$$u = -(\gamma+1)\varkappa\, y\,, \quad v = -(\gamma+1)\varkappa\, x\,.$$

Plugging (5.4) into (5.2) it can be shown (based on the least degeneration principle) that the powers of $u$ and $v$ are balanced in the leading order only when $\beta = 2/3$; in this case the equations for $\varphi(\zeta)$ and $\psi(\zeta)$ become self-similar.

Substituting (5.4) into (5.2$a$), we get the following equation for $\varphi(\zeta)$:‡

$$\left(\beta^2\zeta^3 - 1\right)\frac{d^2\varphi}{d\zeta^2} + \left(\beta(\beta+1)\zeta^2 - \frac{2}{\zeta}\right)\frac{d\varphi}{d\zeta} = 0\,.$$

This is a particular case of a *hypergeometric equation.* Transformation from $\zeta$ to a new variable $z$ defined as (Cole & Cook 1986)

$$z = \left(1 - \beta^2\zeta^3\right)^{-1}\,, \tag{5.5}$$

yields (upon setting $\beta = 2/3$):

$$6z(1-z)\frac{d^2\varphi}{dz^2} + (3 - 11z)\frac{d\varphi}{dz} = 0\,. \tag{5.6}$$

The general solution of equation (5.6) can be expressed via an *incomplete beta function* $B(a,b,z)$ (see Abramovitz & Stegun 1972):

$$\varphi(z) = C_1 + C_2\, B\left(\tfrac{1}{2}, -\tfrac{1}{3}, z\right), \tag{5.7}$$

where $C_1$, $C_2$ are arbitrary constants. For the sake of simplicity we shall employ a shorter notation for the incomplete beta function from (5.7):

$$B(z) \equiv B\left(\tfrac{1}{2}, -\tfrac{1}{3}, z\right) = \int_0^z \frac{d\omega}{\omega^{1/2}(1-\omega)^{4/3}}\,. \tag{5.8}$$

The equation for $\psi(\zeta)$ is obtained by substituting (5.4) into (5.2$b$):

$$\left(\beta^2\zeta^3 - 1\right)\frac{d^2\psi}{d\zeta^2} + \left(\beta(\beta-1)\zeta^2 + \frac{1}{\zeta}\right)\frac{d\psi}{d\zeta} = 0\,,$$

which can be further transformed using (5.5) to get the general solution in terms of $\psi(z)$:

$$\psi(z) = C_3 + C_4\left[B(z) - 3z^{-1/2}(1-z)^{-1/3}\right]\,. \tag{5.9}$$

The four integration constants in the solutions for $\phi$ and $\psi$ are not independent; from

† From now on we are going to neglect the higher order perturbations in (5.4).

‡ Wherever symbol '$\beta$' is used instead of its value 2/3, this is done for the sake of generality; this will also be the case with the parameters $\alpha$ and $\lambda$.

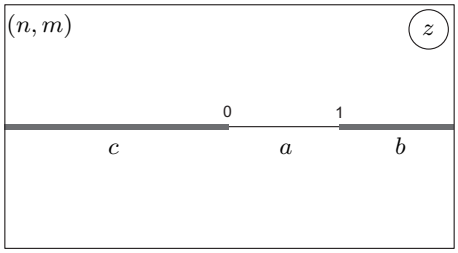


FIGURE 10. A sheet of the Riemann surface for the many-valued functions in (5.10); $a$, $b$, $c$ mark the regions on the real axis which correspond to physically different flow regimes.

(5.1$b$) and (5.4) it follows that $C_1 = C_3$, $C_2 = C_4$, allowing to write the general self-similar solutions for $x$, $y$ in the form

$$y = u\,[C_1 + C_2\,B(z)]\ , \tag{5.10$a$}$$

$$x = v\,\left[C_1 + C_2\left(B(z) - 3z^{-1/2}(1-z)^{-1/3}\right)\right]\ . \tag{5.10$b$}$$

The functions $B(z)$ and $z^{1/2}(1-z)^{1/3}$ are defined on a 6-sheet Riemann surface, with the sheets joined via brunch-cuts $(-\infty, 0)$ (due to $z^{1/2}$) and $(1, \infty)$ (due to $(1-z)^{1/3}$), as shown in Figure 10. Each sheet is characterized by a pair of integer numbers $(n, m)$ denoting brunches of the functions $z^{1/2}$ and $(1-z)^{1/3}$ accordingly, hence taking on the values $n = 1, 2$ and $m = 1, 2, 3$.

Let us describe some basic properties of solutions (5.10). The variable $z$ may be expressed via $u$, $v$ explicitly:

$$z = \left(1 - \beta^2 u^3/v^2\right)^{-1}\ , \tag{5.11}$$

which follows from the definition of $\zeta$ when $\beta = 2/3$. It means that physical solutions correspond to real $z$ and are represented by certain trajectories running along the real axis on the Riemann surface. The branching point $z = 0$ corresponds to $v = 0$ (streamlines in the physical plane reach either a local maximum or a minimum at this point), whereas the branching point $z = 1$ corresponds to the sonic line $u = 0$. From (5.11) it can be seen that subsonic regimes ($u < 0$) are contained in the domain $z \in (0, 1)$, and supersonic regimes are located along the branch cuts $z \in (1, \infty)$ and $z \in (-\infty, 0)$ (regions $a$, $b$ and $c$ in Figure 10, respectively). The latter, obviously, provides stronger supersonic regimes which will be called *supercritical*. Weaker supersonic regimes are located within the branch-cut $z \in (1, \infty)$ and will be called *subcritical*; a connection between these two types of supersonic solutions is made via the point $z = \infty$ achieved when $\zeta^3 = \zeta_c^3$, where $\zeta_c = \beta^{-2/3}$. Using this important value, we can rewrite (5.5) as $z = \left(1 - (\zeta/\zeta_c)^3\right)^{-1}$. The equation $(\zeta/\zeta_c)^3 = 1$ is equivalent to $f^3 = \zeta_c^3\, g^2$, and defines the two lines

$$g = \pm\frac{2}{3}\, f^{\frac{3}{2}} \tag{5.12}$$

in the supersonic part of the phase plane ($f > 0$) (see Figure 11). These lines will be called the *critical lines* as they demarcate sub- and supercritical supersonic regimes, with the latter located within the shaded zone in Figure 11. The upper critical line passes through the node $P_2$, and the lower critical line passes through the saddle point $P_3$.

In the subsequent sections and Part 2 of the work we are going to formulate and prove several important conjectures for the supercritical flow regimes. One of them says that none of the phase trajectories in the $(f, g)$ plane corresponding to solutions (5.10) can

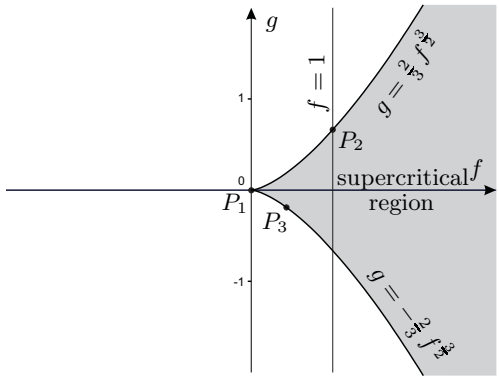


FIGURE 11. Supercritical region in the phase plane.

intersect with the critical lines; the trajectories may at best be tangent to the critical lines or coincide with them. Moreover, if the phase trajectory does not completely coincide with either of the critical lines, then the only possible point of the contact is $P_2$. Hence, if the trajectory starts into the supercritical region, it is guaranteed to stay in it, and passes through the singular line at the only allowed point $P_2$.

The phase variables $f$, $g$ may be expressed via general solutions (5.10) of the inverse problem in the following way:

$$f(z) = \left(\frac{y/u}{x/v}\right)^2 \frac{z-1}{z} \equiv \left(\frac{\varphi(z)}{\psi(z)}\right)^2 \frac{z-1}{z}\,, \tag{5.13a}$$

$$g(z) = \beta\left(\frac{y/u}{x/v}\right)^3 \frac{z-1}{z} \equiv \beta\left(\frac{\varphi(z)}{\psi(z)}\right)^3 \frac{z-1}{z}\,. \tag{5.13b}$$

Thus, there is a link between the self-similar solutions of both the direct and the inverse problems, since $f$ and $g$ can be expressed as functions of either $\xi$ or $z$. Note that the two similarity variables $\xi$ and $\zeta$ are related to one another through

$$\xi^2 = \frac{x^2}{y^3} \equiv \frac{(x/v)^2}{(y/u)^3}\,\frac{v^2}{u^3} = \frac{(x/v)^2}{(y/u)^3}\,\frac{1}{\zeta^3}\,, \tag{5.14}$$

where $x/u$ and $y/u$ again refer to (5.10).

### 5.3. *Boundary conditions in the Inverse problem*

We now need to formulate boundary conditions for the inverse problem in order to find the constants $C_1$, $C_2$ in (5.10). The crucial thing is to determine the values of $z$ which correspond to the physical boundaries $\xi = \pm\infty$. Using the asymptotic form (2.8), we can work out the velocity perturbations $u$ and $v$ in the vicinity of both the upstream and the downstream walls, and plug them into the definition of $\zeta$ to get the relevant values $\zeta_\pm$:

$$\zeta_\pm^3 = \left.\frac{u^3}{v^2}\right|_{\xi\to\pm\infty} = \varkappa_-^2\,\frac{\left(\mp\lambda G_\pm\right)^3}{\varkappa_\pm^2}\,, \qquad \lambda = 3 - \frac{2}{\alpha} = \frac{5}{3}\,.$$

Along with equation (5.11), this yields the required limiting values of $z$:

$$z_- = \left(1 - \beta^2\left(\lambda G_-\right)^3\right)^{-1}, \quad z_+ = \left(1 + \beta^2\left(\lambda G_+\right)^3\left(\varkappa_-/\varkappa_+\right)^2\right)^{-1}, \qquad z_\pm \in \mathbb{R}\,. \tag{5.15}$$

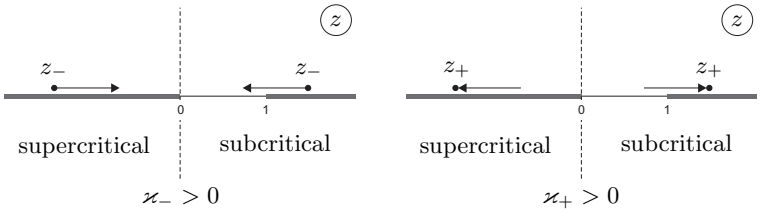


FIGURE 12. Tails of the trajectories in the $z$ plane corresponding to a flow near the upstream wall, left, and the downstream wall, right. The trajectories' direction appears to be the opposite for the subcritical and the supercritical flow regimes.

Hence, the boundary conditions for the inverse problem depend upon the curvatures and the amplitudes of the pressure gradients on either of the walls. These four parameters play the key role in the entire study, and our main task is to find an analytical relationship between them. Equations (5.15) prove the proposals given in section 4.2 (based on the numerical results) for adverse and favourable pressure gradients on both walls. Indeed, if the flow on the upstream wall is subsonic, then $z_- \in (0,1)$, and according to (5.15) $G_- < 0$, which corresponds to a favourable upstream pressure gradient, etc.

To obtain the trajectories representing the flow in the $z$ plane, we first of all need to know the directions in which they emerge from the starting point $z_-$ and return to the final point $z_+$ (running along the real axis in between). These may be obtained from the relationship between the differentials $dz$ and $d\xi$ as $\xi \to \pm\infty$. According to (5.5), $dz = (\beta\zeta)^2 d\zeta^3$; recalling that

$$\zeta^3 = \frac{u^3}{v^2} = \frac{\left(F'\right)^3}{\alpha^2\left(\lambda F - \xi F'\right)^2}\,,$$

and using the asymptotic form (2.8), we arrive at the following equation in the leading order:

$$d\zeta^3 = \pm\frac{C}{\varkappa_\pm}\left[1 - \left(\zeta_\pm/\zeta_c\right)^3\right](\pm\xi)^{-\lambda}d\xi\,, \qquad \xi \to \pm\infty\,, \quad d\xi > 0\,,$$

where

$$C = (\alpha - 1)\left(3\beta\lambda G_\pm\right)^2\left[(\gamma+1)\varkappa_-\right]^{4/3}.$$

Let us assume that on the upstream wall $\varkappa_- > 0$. Thus, the regimes with $\zeta_-^3 < \zeta_c^3$ (oncoming subsonic and subcritical supersonic flows) correspond to $dz < 0$ in the vicinity of $z_-$, and the trajectories in the $z$ plane are leaving to the left of $z_-$. On the contrary, for $\zeta_-^3 > \zeta_c^3$ (oncoming supercritical supersonic flows) we get $dz > 0$: the trajectories in the $z$ plane are leaving to the right of $z_-$ (see Figure 12, left).

If on the downstream wall $\varkappa_+ > 0$ and $\zeta_+^3 < \zeta_c^3$ (the flow is either subsonic or subcritical supersonic), then the trajectories in the $z$ plane are returning towards $z_+$ from the left, whereas for $\zeta_+^3 > \zeta_c^3$ (supercritical supersonic flow) the trajectories are returning towards $z_+$ from the right (see Figure 12, right). However, for concave downstream walls with $\varkappa_+ < 0$ the situation is the opposite, as shown in Figure 13.

It remains to formulate boundary conditions for the functions $x = v\,\psi(z)$ and $y = u\,\varphi(z)$ at $z = z_\pm$. From the boundary condition (2.3) of the direct problem, which has to be modified according to the definition (2.10) of $v$, it follows that

$$y\big|_{z=z_\pm} = 0\,, \quad x\big|_{z=z_\pm} = -\frac{v}{(\gamma+1)\varkappa_\pm}\,. \tag{5.16}$$

Regardless of the flow regime, one can always apply these conditions at one of the two

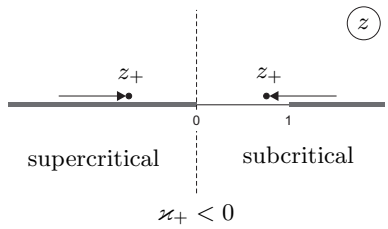


FIGURE 13. Tails of the $z$ plane trajectories corresponding to a flow near a concave downstream wall.

points $z_\pm$ in order to find the constants $C_{1,2}$. Choosing $z_-$ as the starting point and applying (5.16) to (5.10) yields

$$C_1 = -C_2\, B(z_-)\,, \quad C_2 = \frac{z_-^{1/2}\big(1-z_-\big)^{1/3}}{3(\gamma+1)\varkappa_-}\,,$$

leading to the following form of the solutions for $x$, $y$:

$$y = u\,\frac{z_-^{1/2}\big(1-z_-\big)^{1/3}}{3(\gamma+1)\varkappa_-}\Big[B(z)-B(z_-)\Big]\,, \tag{5.17$a$}$$

$$x = v\,\frac{z_-^{1/2}\big(1-z_-\big)^{1/3}}{3(\gamma+1)\varkappa_-}\left[B(z)-\frac{3}{z^{1/2}(1-z)^{1/3}}-B(z_-)\right]. \tag{5.17$b$}$$

Equations (5.17) are valid subject to an appropriate choice of branches for all the complex-valued functions, including $z_-^{1/2}$, $(1-z_-)^{1/3}$ and $B(z_-)$ (functions of the constant $z_-$), and this choice solely depends on the flow regime near the upstream wall. The main criterion is that $x$ and $y$ should always remain real.

Even for the simplest flow regimes the trajectory in the $z$ plane runs on at least two sheets of the Riemann surface, thus requiring to construct regular branches of all the many-valued functions in (5.17). To do this we shall use the standard exponential representation $z = r\,e^{i\vartheta}$, with $-\pi < \vartheta < \pi$ on the sheets $(1,m)$ and $\pi < \vartheta < 3\pi$ on the sheets $(2,m)$. The values $\vartheta = 0,\ 2\pi$ correspond to real positive $z \in (0,\infty)$ (see Figure 14). Similarly, $(1-z) = R\,e^{i\theta}$, with $-\pi < \theta < \pi$ on the sheets $(n,1)$, $\pi < \theta < 3\pi$ on the sheets $(n,2)$ and $3\pi < \theta < 5\pi$ on the sheets $(n,3)$. The values $\theta = 0,\ 2\pi,\ 4\pi$ correspond to real $z \in (-\infty,1)$ (see Figure 14). The arguments $\vartheta$, $\theta$ have been chosen to run through when $z$ moves from one sheet to another because this is convenient for describing transitions between the sheets; however, one can always use local arguments $\bar\vartheta$, $\bar\theta$ which are restricted within $(-\pi,\pi)$ on each sheet, thus giving the following expression for the regular branch of $z^{1/2}(1-z)^{1/3}$ on the sheet $(n,m)$:

$$z^{1/2}(1-z)^{1/3} = r^{1/2}\,R^{1/3}\,\exp\left\{\frac{i\bar\vartheta}{2}+\frac{i\bar\theta}{3}+i\pi(n-1)+\frac{2\pi i}{3}(m-1)\right\}, \tag{5.18}$$

$n = \{1,2\}$, $m = \{1,2,3\}$. Finally, $R$ can be expressed in terms of $r$ for real $z$:

$$R = \begin{cases} 1+r\,, & z \in (-\infty,0)\,,\\ 1-r\,, & z \in (0,1)\,,\\ r-1\,, & z \in (1,\infty)\,. \end{cases} \tag{5.19}$$

Now we have enough tools to analyse the main flow regimes, in the order chosen in section

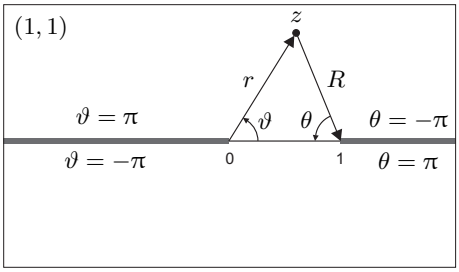


FIGURE 14. Arguments of the complex variables $z$ and $1-z$.

4.2 for the computations. But before that it is worth mentioning some important special cases when solutions (5.17) lead to singularities in the Jacobian (5.3).

### 5.4. *Special cases resulting in a singular Jacobian*

Based upon solutions (5.17) of the inverse problem represented in the form

$$y/u = C\,\varphi\,, \qquad x/v = C\,\psi\,, \tag{5.20}$$

where

$$\varphi(z) = B(z) - B(z_-)\,, \qquad \psi(z) = \varphi(z) - \frac{3}{z^{1/2}(1-z)^{1/3}}\,, \qquad C = \frac{z_-^{1/2}\big(1-z_-\big)^{1/3}}{3(\gamma+1)\varkappa_-}\,,$$

one can easily derive the following expression for the Jacobian (5.3):†

$$J_{uv} = \left|\frac{\partial(x,y)}{\partial(u,v)}\right| = -C^2\left[\left(\varphi - \frac{3z^{1/2}}{(1-z)^{1/3}}\right)^2 + 9(1-z)^{1/3}\right] \equiv z\left(\frac{x}{v}\right)^2(f-1)\,. \tag{5.21}$$

The structure of expressions (5.13) for the phase variables suggests that when $|z|\to\infty$ (with finite $z_\pm$) solutions (5.20) yield the asymptotic forms

$$f = 1 + O\big(r^{-5/6}\big) + O\big(r^{-1}\big)\,, \qquad g = \beta + O\big(r^{-5/6}\big) + O\big(r^{-1}\big)\,, \qquad r = |z| \to \infty\,,$$

i.e. the phase trajectories reach the point $P_2$ on the singular line. Plugging the above expression for $f$ into (5.21), we see that on approaching $P_2$ the Jacobian is estimated as $J_{uv} = O\big(r^{1/6}\big)$, and therefore $J_{uv}\to\infty$. As it was mentioned at the end of section 5.1, an infinite Jacobian does not cause any problems because the functions $x(u,v)$ and $y(u,v)$ are allowed to have multiple values.

However, if the trajectory described by (5.20) crosses the singular line at any point with a finite $z = z_s$ (see Part 2), then from (5.21) it follows that the Jacobian becomes equal to zero, leading to many-valued solutions for $u(x,y)$ and $v(x,y)$. The latter is physically impossible, and makes the crossing illegitimate. This provides an alternative proof that the phase trajectories can only pass through the singular line via the point $P_2$ which corresponds to the limiting characteristic. The two other singularities occurring in (5.21) when $x\to 0$ and $v\to 0$ are removable since in these cases $f\sim x^{-2}$ and $z\sim v^2$, respectively.

The Jacobian may also be represented in terms of the phase variables only: ‡

$$J_{uv} = \frac{y^{6-4\alpha}}{\alpha^4\xi^4(\alpha-1)^2}\left[\frac{f-1}{9g^2-4f^3}\right]\,.$$

† We used expression (5.13) for $f$ to obtain the last equality.
‡ Note that $J_{uv}$ becomes self-similar when $\alpha = 3/2$.

From this it follows that on both critical lines, defined in (5.12), $J_{uv} = \infty$. Therefore, in the case when a phase trajectory coincides with one of the critical lines, solutions (5.20) do not work, and we have to solve the direct problem (section 5.7).

Finally, an immediate connection between the self-similar solutions of the direct and the inverse problems (the latter given by (5.20)) is described by the one-dimensional Jacobian

$$\frac{d\xi}{d\zeta} = \frac{\beta\, u\, z}{y^{1/2}\, v^{1/3}} \left[\frac{f-1}{f}\right],$$

which has only one non-trivial singularity when $f = 1$ for a finite $z$, again referring to the illegitimate crossing of the singular line (the singularity associated with the branching point $z = 0$ is eliminated by moving the trajectory to the next sheet of the Riemann surface, see section 5.5). In other words, whenever the Jacobian $d\xi/d\zeta$, treated as a function of $z$, becomes zero at any finite point of the trajectory in the $z$ plane (except for the origin), the transformation $\xi(\zeta)$ is no longer monotonic, thus creating physically impossible multiple values in the functions $u(x, y)$ and $v(x, y)$.†

We shall now move on to describe all the possible transonic local flow regimes which can develop near the curvature break.

### 5.5. *Subsonic flow on the upstream wall*

In section 5.2 it was shown that subsonic flows correspond to $z \in (0, 1)$. Hence, for the regime considered in this section, the upstream boundary conditions are applied at $z_- \in (0, 1)$, and the trajectory leaves to the left of this point towards $z = 0$, due to the property discussed in 5.4. To make general solutions (5.17) real in the subsonic region, one needs to use the branch with $n = 1$, $m = 1$ of the function $z^{1/2}(1 - z)^{1/3}$ (see 5.18). Since $\vartheta = \theta = 0$ for $z \in (0, 1)$, equations (5.18), (5.19) yield

$$z^{1/2}(1-z)^{1/3} = r^{1/2}(1-r)^{1/3}, \qquad 0 < r < 1\,.$$

The function $B(z)$ contains exactly the same regular branch and is real:

$$B(z) \equiv B(r) = \int_0^r \frac{d\rho}{\rho^{1/2}(1-\rho)^{4/3}}, \qquad \rho \in \mathbb{R}\,;$$

this is also true for the coefficient $z_-^{1/2}\big(1 - z_-\big)^{1/3}$, in which $z_-$ can simply be replaced by $r_-$. Applying these results to (5.17), we get the following solutions in the vicinity of the upstream wall:

$$y = u\,\frac{r_-^{1/2}\big(1-r_-\big)^{1/3}}{3(\gamma+1)\varkappa_-}\Big[B(r) - B(r_-)\Big], \tag{5.22$a$}$$

$$x = v\,\frac{r_-^{1/2}\big(1-r_-\big)^{1/3}}{3(\gamma+1)\varkappa_-}\left[B(r) - \frac{3}{r^{1/2}(1-r)^{1/3}} - B(r_-)\right]. \tag{5.22$b$}$$

Since

$$\frac{dB(r)}{dr} = \frac{1}{r^{1/2}(1-r)^{4/3}} \geqslant 0\,, \qquad 0 < r < 1\,,$$

$B(r)$ grows steadily with $r$. Together with the inequality $u < 0$ valid for all subsonic flows and (5.22$a$), this implies that the restriction $y \geqslant 0$ holds for $0 < r \leqslant r_- < 1$, which means that the trajectory in the $z$ plane indeed goes to the left of $r_-$. At the same time (5.22$b$) gives $x < 0$ when $v > 0$, which is, indeed, the case near a convex upstream wall.

† The point $z = \infty$ is excluded because it corresponds to the removable singularity associated with the limiting characteristic.

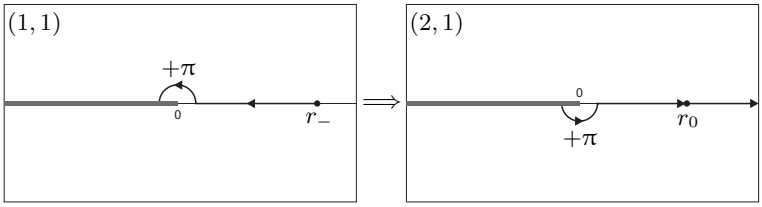


FIGURE 15. First two fragments of the $z$ plane trajectory for an oncoming subsonic flow. The sign of $v$ changes as the trajectory makes a complete turnover around the branching point $z = 0$ and finds itself on the next sheet of the Riemann surface. This is followed by the change of sign of $x$ when $z = r_0$.

Once the trajectory has left the point $r_-$, its further behaviour in the $z$ plane is quite obvious. First of all, the trajectory cannot turn backwards at any regular point because the transformation $\xi(z)$, as expected, appears to be monotonic for solutions (5.22) (see end of section 5.4). Hence, the trajectory goes towards the origin $z = 0$ (which is also the branching point of function $z^{1/2}$). When $z = 0$ is reached, it means that $v = 0$ and the sign of $v$ is to be changed, as it can be seen from the relevant computations in section 4.2 (Figure 4). Without a loss of generality, one can say that the change of the sign leads to $\Delta \arg v = +\pi$. Writing the Taylor expansion of (5.11) when $v \to 0$, $u \neq 0$ yields

$$z = -\frac{v^2}{\beta^2 u^3}\left(1 + O(v^2)\right) .$$

Therefore, the change in sign of $v$ corresponds to $\Delta \arg z = +2\pi$, which means that the trajectory makes a single turnover along an infinitesimal circle around the point $z = 0$, and finds itself in the subsonic region on the sheet $(2, 1)$, as shown in Figure 15.

There is a theoretical explanation for the fact that $v$ must change sign, based upon the following requirements: a $z$ plane trajectory should always remain on the real axis and cannot turn backwards at any point, while the corresponding solutions for $x$ and $y$, given by (5.22), should be real for all values of $z$ along the trajectory. The only possibility for a trajectory to comply with these requirements is to make a single turnover around the origin and find itself in the subsonic region on the second sheet of the function $z^{1/2}$. Moreover, the above arguments suggest that a flow which is originally subsonic or subcritical supersonic cannot accelerate to become supercritical supersonic. Should this happen, solutions (5.22) would lead to complex $x$ and $y$. Due to the same reason supercritical flows cannot decelerate to subcritical supersonic or subsonic speeds. The latter also means that for supercritical supersonic flows the phase trajectories always remain in the supercritical region (Figure 11) unless the flow undergoes a shock, and the relevant trajectories in the $z$ plane have to stay within the branch-cut $-\infty < z \leqslant 0$.

In the subsonic region on the sheet $(2, 1)$, according to (5.18) and (5.19), $z^{1/2} = -r^{1/2}$, $(1 - z)^{1/3} = (1 - r)^{1/3}$, and from (5.8) $B(z) = -B(r)$. Hence, the turnover transforms solutions (5.22) into

$$y = -u\,\frac{r_-^{1/2}\left(1 - r_-\right)^{1/3}}{3(\gamma + 1)\varkappa_-}\left[B(r) + B(r_-)\right] , \tag{5.23a}$$

$$x = v\,\frac{r_-^{1/2}\left(1 - r_-\right)^{1/3}}{3(\gamma + 1)\varkappa_-}\left[\frac{3}{r^{1/2}(1 - r)^{1/3}} - \left(B(r) + B(r_-)\right)\right] . \tag{5.23b}$$

These are the analytical continuations of (5.22) through the singular point $z = 0$ in the equations for $\varphi(z)$ and $\psi(z)$ (see (5.6)). The singularity is trivial, because the relevant

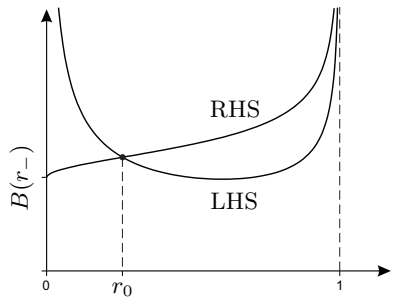


FIGURE 16. Left-hand side (LHS) and right-hand side (RHS) of the transcendental equation (5.24) plotted as functions of $r_0$.

solutions in the physical plane are regular near the line $v = 0$, and is simply due to the transformation of the variables associated with the inverse problem.

After the turnover, the trajectory in the $z$ plane leaves to the right of $z = 0$ and travels towards $z = 1$ (see Figure 15) as $\xi(z)$, according to (5.14), continues to grow when $r$ is increasing in (5.23). Solution (5.23$a$) for $y$ is guaranteed to be positive for $0 < r < 1$ because $u < 0$. However, solution (5.23$b$) for $x$ changes its sign from negative to positive at some point $r_0 \in (0, 1)$ which satisfies the transcendental equation

$$B(r_0) + B(r_-) = 3r_0^{-1/2}\big(1 - r_0\big)^{-1/3}. \tag{5.24}$$

The latter has a clear graphic solution for certain values of the parameter $r_-$ (see Figure 16). This solution appears to be unique and exists when $r_- \in (r_*, 1)$, with $r_* \approx 0.3039$ being the only root of the equation

$$B(r_*) = \frac{3\sqrt{\pi}\,\Gamma(2/3)}{\Gamma(1/6)}, \tag{5.25}$$

where $\Gamma(s)$ is the Euler's *Gamma function*.† The corresponding trajectory in the phase plane stretches into infinity when $r \to r_0^-$, and reflects itself from the $g = 0$ axis when $x$ changes sign (Figure 4).

Upon passing through $r_0$, the trajectory in the $z$ plane approaches the branching point $z = 1$ on the sheet $(2, 1)$. This branching point corresponds to the sonic line ($u = 0$). From the numerical solution we already know that the phase trajectories cross this line and enter the supersonic region, i.e. $u$ needs to change sign once the sonic point $z = 1$ is reached in the plane of complex $z$. Applying the Taylor expansion to (5.11) when $u \to 0$, $v \neq 0$ yields

$$z = 1 + \frac{\beta^2 u^3}{v^2} + O(u^6).$$

Hence, the change in sign of $u$, which can be expressed as $\Delta \arg u = +\pi$ without a loss of generality, results in $\Delta \arg(1 - z) = +3\pi$. The latter is equivalent to the trajectory making one and a half revolutions along an infinitesimal circle around $z = 1$, finding itself at the lower side of the branch cut $(1, \infty)$ on the sheet $(2, 2)$, as shown in Figure 17.‡

To continue the function $B(z)$ analytically through singular point $z = 1$, we use its

† Equation (5.25) follows from the asymptotic behaviour of $B(z)$ when $z \to 1^-$.

‡ Again, there is a theoretical explanation for this, similar to the one given previously for the change in sign of $v$.

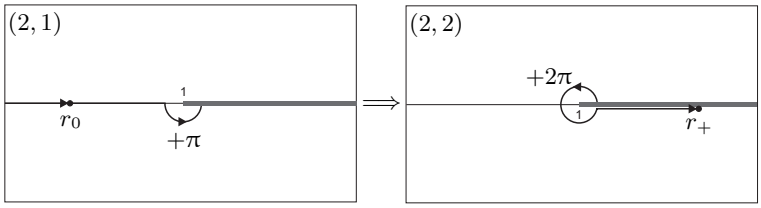


FIGURE 17. Final fragments of the $z$ plane trajectory for an oncoming subsonic flow. The branching point $z = 1$ corresponds to the sonic line ($u = 0$).

equivalent representation on the sheet $(n, m)$:¶

$$B(z) = (-1)^n \frac{3\sqrt{\pi}\,\Gamma(2/3)}{\Gamma(1/6)} + \frac{3}{2}\int_1^z \frac{d\omega}{\omega^{3/2}(1-\omega)^{1/3}} + \frac{3}{z^{1/2}(1-z)^{1/3}}\,. \tag{5.26}$$

Setting $n = m = 2$, $\widetilde{\vartheta} = 0$, $\widetilde{\theta} = \pi$ in (5.18), (5.19) and substituting the results into (5.26) gives the real expression for $B(z)$ at the lower side of the branch cut $(1, \infty)$ on the sheet $(2, 2)$

$$B(z) = \frac{3\sqrt{\pi}\,\Gamma(2/3)}{\Gamma(1/6)} + \frac{3}{2}\int_1^r \frac{d\rho}{\rho^{3/2}(\rho-1)^{1/3}} + \frac{3}{r^{1/2}(r-1)^{1/3}}\,, \qquad \rho \in \mathbb{R}\,, \quad 1 < r < \infty\,.$$

With this expression in mind, one can write down the solutions for $x$, $y$ in this region, describing a subcritical supersonic flow:

$$y = u\,\frac{r_-^{1/2}\big(1-r_-\big)^{1/3}}{3(\gamma+1)\varkappa_-}\left[-B(r_-) + \frac{9\sqrt{\pi}\,\Gamma(2/3)}{\Gamma(1/6)} + I(r)\right], \tag{5.27a}$$

$$x = v\,\frac{r_-^{1/2}\big(1-r_-\big)^{1/3}}{3(\gamma+1)\varkappa_-}\left[-B(r_-) + \frac{9\sqrt{\pi}\,\Gamma(2/3)}{\Gamma(1/6)} + I(r) - \frac{3}{r^{1/2}(r-1)^{1/3}}\right], \tag{5.27b}$$

where

$$I(r) = \int_r^\infty \frac{d\rho}{\rho^{1/2}(\rho-1)^{4/3}}\,, \qquad 1 < r < \infty\,.$$

Now we have $u > 0$, $v < 0$. Again, the functions in (5.27) are the analytical continuations of (5.23) through the singular point $z = 1$.

In order to provide a monotonic increase of $\xi$ with $x$ and $y$ given by (5.27), the trajectory in the $z$ plane has to move further to the right of $z = 1$ along the branch cut. It can be easily proved that $x$ remains positive when $r$ is increasing, whereas $y$ becomes zero at some finite point $r_+ > 1$ corresponding to the downstream wall (see Figure 17).† Applying boundary conditions (5.16) to (5.27) at this point, we arrive at the following algebraic system of two equations:

$$B(r_-) = \frac{9\sqrt{\pi}\,\Gamma(2/3)}{\Gamma(1/6)} + I(r_+)\,, \tag{5.28a}$$

$$\frac{\varkappa_+}{\varkappa_-} = \frac{r_+^{1/2}\big(r_+-1\big)^{1/3}}{r_-^{1/2}\big(1-r_-\big)^{1/3}}\,. \tag{5.28b}$$

¶ This formula implies using expression (5.18) for $z^{1/2}(1-z)^{1/3}$ and $\omega^{1/2}(1-\omega)^{1/3}$ on the sheet $(n, m)$.

† Note that the trajectory returns to $r_+$ from the left, in agreement with the general rule derived earlier.

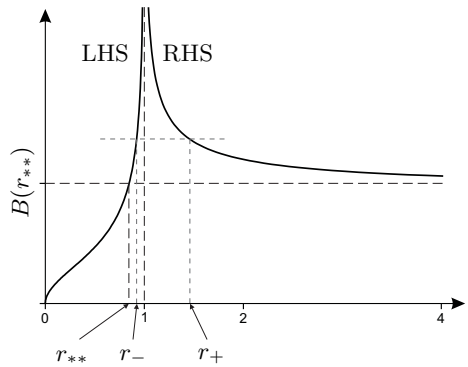


FIGURE 18. Left-hand side (LHS) and right-hand side (RHS) of (5.28$a$), plotted as functions of $r_-$ and $r_+$ respectively.

These equations allow to determine any two of the three parameters $r_-$, $r_+$, $\varkappa_+/\varkappa_-$ for a given value of the third one. The most physically meaningful case is when the curvatures ratio $\varkappa_+/\varkappa_-$ is known and $r_\pm$ are expressed as functions of it, yielding the coefficients $G_\pm$ related to the wall pressure gradients.

Let us discuss some basic properties of equations (5.28). First of all, (5.28$a$) implicitly sets a functional dependence $r_+(r_-)$ (or vice versa) and admits the limit

$$r_- \to 1^-\,, \quad r_+ \to 1^+\,,$$

where the "rate of the approach" is the same from both sides:

$$\lim_{r_-\to 1^-}\left[\frac{r_+(r_-)-1}{1-r_-}\right] = 1\,.$$

This limit corresponds to $\varkappa_+/\varkappa_- \to 1$ due to (5.28$b$), and reduces solutions (5.22), (5.23), (5.27) to $y = -u/\left((\gamma+1)\varkappa\right)$, $x = -v/\left((\gamma+1)\varkappa\right)$, where $\varkappa = \varkappa_- = \varkappa_+$. The flow described by these linear functions is nothing else than a potential vortex outside a convex cylindrical surface (with no curvature break), and is related to the simple analytical solution $F(\xi) = -(\gamma+1)\varkappa\xi$ of the direct problem, thus being an important reference point for the whole study. One of the properties of this flow is that there is no pressure gradient on both walls in the leading order, i.e. $G_\pm = 0$.

Secondly, system (5.28) also admits the limit $r_+ \to \infty$, for which $r_-$ tends to a finite value $r_{**} \approx 0.8302$, the latter being the only root of the transcendental equation

$$B(r_{**}) = \frac{9\sqrt{\pi}\,\Gamma(2/3)}{\Gamma(1/6)}\,. \tag{5.29}$$

This property is illustrated graphically in Figure 18, where the left-hand side of (5.28$a$) is plotted as a function of $r_-$, and the right-hand side of (5.28$a$) – as a function of $r_+$. Hence, we get the important restriction for the possible values of $r_-$ within this particular flow regime:

$$r_{**} < r_- \leqslant 1\,. \tag{5.30}$$

As $r_+$ increases from $1^+$ to $\infty$, $r_-$ decreases steadily from $1^-$ to $r_{**}$ (because both curves plotted in Figure 18 are monotonic functions of their arguments). Applying this result to (5.28$b$), it can be shown that $\varkappa_+/\varkappa_-$ increases monotonously from 1 to $\infty$ with $r_+$, thus covering all the possible values of the curvatures ratio for the oncoming subsonic flows. Essentially, the upstream flow is subsonic whenever $\varkappa_+/\varkappa_- > 1$, i.e. when the

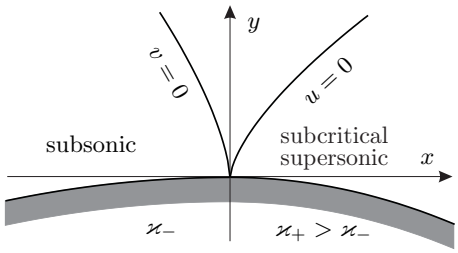


FIGURE 19. Regime with a subsonic flow near the upstream wall.

upstream wall is flatter compared to the downstream wall.† The limiting value $G_{min}$ of the upstream pressure gradient discovered in section 4.2 numerically is then given by

$$G_{min} = \lim_{r_- \to r_{**}^+} G_- = -\frac{1}{\lambda \beta^{2/3}} \left[ \frac{1 - r_{**}}{r_{**}} \right]^{1/3} ,$$

according to (5.15).

The relevant flow structure in the physical plane is shown in Figure 19. The oncoming subsonic flow (i.e., the subsonic flow near the upstream wall) firstly passes through the line where $v = 0$, and the streamlines reach a local maximum; this line corresponds to

$$\xi = \xi \big|_{v=0} = -\frac{2}{\big[B(r_-)\big]^{\frac{3}{2}}} \left( \frac{3(\gamma+1)\varkappa_-}{r_-^{1/2}\big(1 - r_-\big)^{1/3}} \right)^{1/2} .$$

The flow then passes through the symmetry axis $x = 0$ and accelerates, transforming to a subcritical supersonic flow; this transition takes place at the sonic line with the position

$$\xi = \xi \big|_{u=0} = \beta \left[ \frac{1}{3} B(r_-) - \frac{\sqrt{\pi}\,\Gamma(2/3)}{\Gamma(1/6)} \right] \left( \frac{(\gamma+1)\varkappa_-}{r_-^{1/2}\big(1 - r_-\big)^{1/3}} \right)^{1/2} .$$

The subcritical supersonic flow occupies the entire space between the sonic line and the downstream wall (Figure 19).

For the particular flow regime described in this section, the two following limiting cases prove to be important and can be studied analytically:

$$\frac{\varkappa_+}{\varkappa_-} = 1 + \varepsilon \,, \qquad \frac{\varkappa_+}{\varkappa_-} = \frac{1}{\varepsilon} \,,$$

where $0 < \varepsilon \ll 1$. They were described in detail by Yumashev (2010). The first case allows to study the onset of boundary-layer separation analytically, while the second one provides important link between the transonic Prandtl-Meyer flow (section 5.7) and various other flow regimes. These results are summarized in Part 2.

### 5.6. *Subcritical supersonic flow on the upstream wall*

The phase trajectories obtained for the oncoming subsonic flows can be run in the opposite direction, because they stay within the subcritical zone and do not develop discontinuities (except for the trivial jump at $\xi = 0$). Indeed, the substitution $\xi \to -\xi$ does not change the variable $\chi$ in (3.4), and any continuous trajectory described by autonomous

† For certain supercritical supersonic flows the curvatures ratio may also be greater than one, although the wall pressure gradients would be completely different (Part 2).

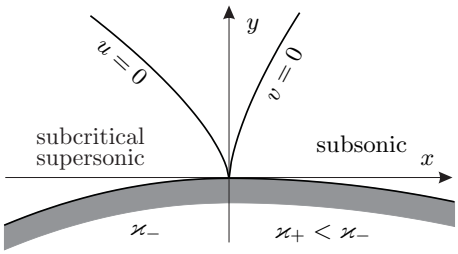


FIGURE 20. Regime with a subcritical supersonic flow near the upstream wall.

system (3.5) can be run in both directions while $\xi$ changes from $-\infty$ to $\infty$. These arguments suggest that there should exist a regime which is symmetrical with respect to the oncoming subsonic flow, i.e. with a subcritical supersonic flow on the upstream wall decelerating to subsonic speeds without a shock formation. From the reflection rule it follows that such a flow would exist when $0 < \frac{\varkappa_+}{\varkappa_-} < 1$ (flatter downstream wall).‡

Mathematically the reflection requires the following substitutions in all the analytical solutions derived for the subsonic upstream flows in section 5.5:

$$r_- \longleftrightarrow r_+ \,, \qquad \varkappa_- \longleftrightarrow \varkappa_+ \,.$$

Now $r_- \in (1, \infty)$, $r_+ \in (r_{**}, 1)$, and the trajectory in the $z$ plane travels in the opposite direction. The whole flow pattern (Figure 20) again comprises of three regions, and is symmetrical to that obtained in section 5.5 with respect to the $x = 0$ line; the relevant analytical solutions resemble (5.22), (5.23), (5.27) (Yumashev 2010), and are not listed here for the sake of brevity. Applying the boundary conditions, one gets the system of two algebraic equations similar to (5.28):

$$B(r_+) = \frac{9\sqrt{\pi}\,\Gamma(2/3)}{\Gamma(1/6)} + I(r_-)\,, \tag{5.31$a$}$$

$$\frac{\varkappa_+}{\varkappa_-} = \frac{r_+^{1/2}\big(1 - r_+\big)^{1/3}}{r_-^{1/2}\big(r_- - 1\big)^{1/3}}\,. \tag{5.31$b$}$$

As before, this system allows to determine the parameters $r_\pm$ for a given ratio of the curvatures, and has the same properties as (5.28) (in particular, the two limiting cases mentioned in section 5.5). The curvatures ratio is now changing between $1^-$ (when $r_- = 1^+$, $r_+ = 1^-$) and $0^+$ (when $r_- \to \infty$, $r_+ \to r_{**}^+$).

Solving (5.31) numerically with respect to $r_\pm$ yields the coefficients $G_\pm$ as functions of the curvatures ratio; these are plotted in Figure 8. This time the pressure gradients on both walls are adverse (and singular), and a boundary layer separation is expected to take place for this regime. The limiting value $G_{max}$ of the upstream pressure gradient discovered in section 4.2 numerically is given by

$$G_{max} = \lim_{r_- \to \infty} G_- = \frac{1}{\lambda \beta^{2/3}} > |G_{min}|\,,$$

which follows from (5.15). In Figure 21 the gradients ratio is shown as a function of the curvatures ratio when $0 < \frac{\varkappa_+}{\varkappa_-} < 1$; this graph is obviously the inversion of Figure 6 plotted for $1 < \frac{\varkappa_+}{\varkappa_-} < \infty$.

‡ This result was also obtained in the computations, see section 4.2.

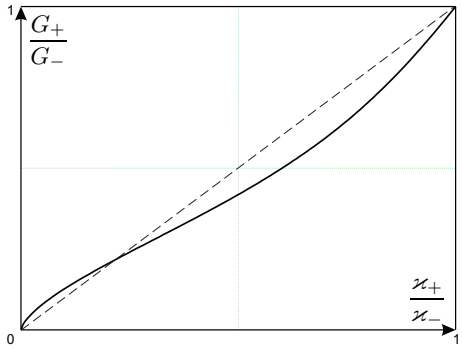


FIGURE 21. The ratio of the gradients plotted verses the ratio of the curvatures when $0 < \frac{\varkappa_+}{\varkappa_-} < 1$.

### 5.7. *Transonic Prandtl–Meyer flow*

Let us now consider the limiting case $\frac{\varkappa_+}{\varkappa_-} = \varepsilon \to 0$ (interpreted as $\varkappa_- = O(1)$, $\varkappa_+ \to 0^+$ for the oncoming supersonic flow), which is symmetrical to the limit $\frac{\varkappa_+}{\varkappa_-} = \frac{1}{\varepsilon}$ mentioned in section 5.5. Now $r_- \to \infty$, $r_+ \to r_{**}^+$, and the Jacobian (5.3) tends to infinity as $r \to \infty$ (Yumashev 2010). It means that the inverse transformation $(u, v) \to (x, y)$ is not uniquely defined, and one has to solve the direct problem (either for $F(\xi)$ or for $f(\xi)$, $g(\xi)$).

To understand this limiting case better, we need to look at the behaviour of the corresponding phase trajectories. For small $\varkappa_+/\varkappa_-$ the trajectory, after leaving the origin, is located slightly below the lower critical line $g = -\frac{2}{3} f^{\frac{3}{2}}$ in the supersonic region. When approaching the saddle point $P_3$, it abruptly turns to the left and moves towards the subsonic region, as shown in Figure 7. However, in the limit $\varkappa_+/\varkappa_- \to 0$ the trajectory merges with the lower critical line, being confined within the fragment of the line between the origin and the saddle point (Figure 7, trajectory $d$). The Jacobian is equal to $\infty$ on the critical lines, and, as already mentioned above, in this case one has to solve the direct problem. The relevant solution for $f(\xi)$ can be obtained analytically (Yumashev 2010).

From the local analysis of the trajectory's behaviour in the vicinity of the saddle point one can find that the critical line $g = -\frac{2}{3} f^{\frac{3}{2}}$ coincides with the second half-line of the saddle (see end of section 3.2). Moreover, the trajectory arrives to the saddle point strictly when $\xi = 0$; all other trajectories, which do not coincide with the lower critical line, either turn to the left (subcritical supersonic flows) or to the right (supercritical supersonic flows) when approaching the saddle point, as shown in Figure 7. Hence, the point acts as a switch between two physically different regimes. The only trajectory coinciding with the lower critical line may therefore be called the *critical trajectory*, and the relevant solution for $f(\xi)$ describes the transonic Prandtl–Meyer compression wave (Liepmann & Roshko 1957).†

Once this phase trajectory reaches the saddle point, it cannot go further along the critical line as this would lead to an illegitimate intersection with the singular line $f = 1$. Instead, the trajectory jumps back into the origin and stays there for all $\xi \in (0, \infty)$, thus giving a uniform flow with $u = v = 0$ above the flat downstream wall (see Figure 5.7). The jump leads to a weak discontinuity along the $x = 0$ line in the physical plane; namely,

† A very similar flow regime was also discovered by Ruban *et al.* (2006), who studied inviscid transonic flow near a different kind of singularity in wall curvature.

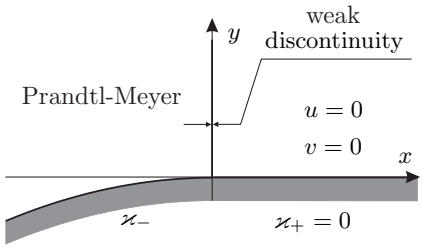


FIGURE 22. Local structure of the flow in the case of a flat downstream wall.

the second derivatives of the velocity components are broken, which can easily be verified from the solution for $F(\xi)$ near the saddle point (Yumashev 2010).

The downstream wall pressure gradient (proportional to $G_+$) is obviously zero in the uniform flow over a flat downstream wall. By applying the limit $\varkappa_+/\varkappa_- \to 0$ to the flow regime described in section 5.6 it can be shown that

$$\lim_{\varkappa_+\to 0}\left[\frac{G_+}{\varkappa_+^{2/3}}\right] = \frac{1}{\lambda}\left(\frac{1}{\beta\varkappa_-}\right)^{2/3}\left(\frac{1-r_{**}}{r_{**}}\right)^{1/3}, \qquad \varkappa_- = O(1)\,,$$

with $r_{**}$ defined in (5.29). Thus, $G_+ \sim \varkappa_+^{2/3} \to 0$ when $\varkappa_+ \to 0$.

All these results are symmetric to the limiting case of $\varkappa_- = 0$, $\varkappa_+ = O(1)$ mentioned in the end section 5.5. This is, in fact, the last regime with the reversibility property with respect to the transformation $x \to -x$.

### 5.8. *Supercritical supersonic flow on the upstream wall*

The next regime to follow (when the phase trajectory is slightly above the critical line and turns to the right upon passing by the saddle point, as shown in Figure 9) involves supercritical supersonic flows. Such flows pass through the limiting characteristic and inevitably develop a shock wave; therefore, they cannot be inverted. This will be described in detail in Part 2.

## 6. Conclusions

We have considered an inviscid transonic flow in the vicinity of a curvature break (assuming the boundary-layer separation is local). This analysis revealed a complicated physical picture of the flow depending on the ratio of the curvatures. In particular, we observed a certain type of supersonic flows which decelerate to subsonic speeds without a shock wave, transonic Prandtl–Meyer flow and supersonic flows with a weak shock.† From an asymptotic analysis of the Karman–Guderley equation it was demonstrated that the curvature discontinuity leads to the singular pressure gradients $\partial p/\partial s \sim G_\mp\,(\mp s)^{-1/3}$ upstream and downstream of the break point, respectively. In order to find the amplitude coefficients $G_\mp$, we performed computations based on a new numerical technique of integrating the ODE form of the Karman–Guderley equation. The computational results were then explained theoretically using the *hodograph method* along with the *phase portrait* of the flow.

† It will be shown in Part 2 that extending the flow beyond the *limiting characteristic* is both the necessary and the sufficient condition of a shock formation. As a consequence, a fundamental link between the local and the global flow patterns is observed in our problem, and if the local flow with a shock is to be defined uniquely, one extra parameter (in addition to the ratio of the curvatures) needs to be specified.

The author would like to acknowledge the useful comments and suggestions of Professor A. Ruban. The study was performed in 2007 as part of a PhD research project supported by the ORS Awards Scheme and the scholarship from the School of Mathematics, University of Manchester.

## REFERENCES

Abramovitz, M & Stegun, I A 1972 *Handbook Of Mathematical Functions With Formulas, Graphs, And Mathematical Tables*, 9th edn. Wiley-Interscience.

Bogdanov, A., Diesperov, V., Zhuk, V. & Chernyshev, A. 2010 Triple-deck theory in transonic flows and boundary layer stability. *Computational Mathematics and Mathematical Physics* **50**, 2095–2108.

Buldakov, E V & Ruban, A I 2002 On transonic viscous-inviscid interaction. *J. Fluid Mech.* **470**, 291–317.

Chaplygin, S 1902 Gas Jets. *Scientific Memoirs, Moscow University* .

Cole, J D & Cook, L P 1986 *Transonic Aerodynamics*. Elsevier Science Publishers B.V.

Frankl, F I 1947 Studies in the theory of infinite aspect ratio wing moving with the speed of sound. *Dokl. Akad. Nauk SSSR* **57** (7), 1561–1564.

Guderley, G 1957 *Theorie Schallnahe Stromungen.*. Springer-Verlag Berlin, english translation: Addison-Wesley 1962.

Landau, L D & Lifshitz, E M 1959 *Fluid Mechanics.*. Pergamon Press.

Liepmann, H W & Roshko, A 1957 *Elements of Gasdynamics.*. John Wiley & sons, New York.

Messiter, A F & Hu, J J 1975 Laminar boundary layer at a discontinuity in wall curvature. *Q. Appl. Math.* **33** (3), 175–181.

Neiland, V Ya 1974 *Asymptotic problems in the theory of viscous supersonic flows.*. Tr. TsAGI.

Ruban, A I 1974 On laminar separation at a corner point on a solid surface. *Uch. zap. TsAGI* **5** (2), 44–54.

Ruban, A I & Turkyilmaz, I 2000 On laminar separation at a corner point in transonic flow. *J. Fluid Mech.* **423**, 345–380.

Ruban, A I, Wu, X & Pereira, R M S 2006 Viscous-inviscid interaction in transonic prandtl-meyer flow. *J. Fluid Mech.* **568**, 387–424.

Sychev, V V, Ruban, A I, Sychev, Vik V & Korolev, G L 1998 *Asymptotic Theory Of Separated Flows*. Cambridge University Press.

Yumashev, D. 2010 Viscous-inviscid interaction in a transonic flow caused by a discontinuity in wall curvature. PhD thesis, University of Manchester.